Enzymatic toxins from snake venom: structural characterization and mechanism of catalysis

Tse Siang Kang[1], Dessislava Georgieva[2], Nikolay Genov[3], Mário T. Murakami[4], Mau Sinha[5], Ramasamy P. Kumar[5], Punit Kaur[5], Sanjit Kumar[5], Sharmistha Dey[5], Sujata Sharma[5], Alice Vrielink[6], Christian Betzel[2], Soichi Takeda[7], Raghuvir K. Arni[8], Tej P. Singh[5] and R. Manjunatha Kini[9]

1 Department of Pharmacy, National University of Singapore, Singapore
2 Institute of Biochemistry and Molecular Biology, University of Hamburg, Laboratory of Structural Biology of Infection and Inflammation, Germany
3 Institute of Organic Chemistry, Bulgarian Academy of Sciences, Sofia, Bulgaria
4 National Laboratory for Biosciences, National Center for Research in Energy and Materials, Campinas, Brazil
5 Department of Biophysics, All India Institute of Medical Sciences, New Delhi, India
6 School of Biomedical, Biomolecular and Chemical Sciences, University of Western Australia, Crawley, Australia
7 National Cerebral and Cardiovascular Center Research Institute, Suita, Osaka, Japan
8 Department of Physics, Centro Multiusuário de Inovação Biomolecular, São Paulo State University, São José do Rio Preto, Brazil
9 Department of Biological Sciences, Protein Science Laboratory, National University of Singapore, Singapore

Snake venoms are cocktails of enzymes and non-enzymatic proteins used for both the immobilization and digestion of prey. The most common snake venom enzymes include acetylcholinesterases, L-amino acid oxidases, serine proteinases, metalloproteinases and phospholipases A$_2$. Higher catalytic efficiency, thermal stability and resistance to proteolysis make these enzymes attractive models for biochemists, enzymologists and structural biologists. Here, we review the structures of these enzymes and describe their structure-based mechanisms of catalysis and inhibition. Some of the enzymes exist as protein complexes in the venom. Thus we also discuss the functional role of non-enzymatic subunits and the pharmacological effects of such protein complexes. The structures of inhibitor–enzyme complexes provide ideal platforms for the design of potent inhibitors which are useful in the development of prototypes and lead compounds with potential therapeutic applications.

Introduction

Snakes have fascinated mankind since prehistoric times. They are one of the few living organisms which evoke a response – positive or negative – when one hears a hissing or rattling sound or even a mere mention of the word 'snake'. This intense fascination probably arises from the deadly effect of their venoms, which when

Abbreviations

ACh, acetylcholine; AChE, acetylcholinesterase; ADAM, a disintegrin and metalloproteinase; ADAMTS, ADAM with thrombospondin type-1 motif; β-BTx, β-bungarotoxin; CAS, catalytic anionic site; DAAO, D-amino acid oxidase; FXa, factor Xa; HVR, hyper-variable region; LAAO, L-amino acid oxidase; MDC, metalloproteinase/disintegrin/cysteine-rich; NSAIDs, non-steroidal anti-inflammatory drugs; PAS, peripheral anionic site; PDB, Protein Data Bank; PLA$_2$, phospholipase A$_2$; RVV-X, Russell's viper venom FX activator; SVSP, snake venom serine proteinase; TSV-PA, *Trimeresurus stejnegeri* venom plasminogen activator; VAP, vascular apoptosis-inducing protein.

injected into the victim cause a variety of physiological reactions such as paralysis, myonecrosis and often death. Snake venoms have evolved into complex mixtures of pharmacologically active proteins and peptides that exhibit potent, lethal and debilitating effects to assist in prey capture. Their diet is very varied and includes small animals, snails, fishes, frogs, toads, lizards, chickens, mice, rats and even other snakes. Human envenomation is rare and unfortunate. Snakes use their venoms as offensive weapons in incapacitating and immobilizing their prey (the primary function), as defensive tools against their predators (the secondary function) and to aid in digestion. Biochemically, snake venoms are complex mixtures of pharmacologically active proteins and polypeptides. All of them in concert help in immobilizing the prey. A large number of protein toxins have been purified and characterized from snake venoms [1,2] and snake venoms typically contain from 30 to over 100 protein toxins. Some of these proteins exhibit enzymatic activities, whereas several others are non-enzymatic proteins and polypeptides. Based on their structures, they can be grouped into a small number of toxin superfamilies. The members in a single family show remarkable similarities in their primary, secondary and tertiary structures but they often exhibit distinct pharmacological effects.

The most common enzymes in snake venoms are phospholipase A$_2$s (PLA$_2$s), serine proteinases, metalloproteinases, acetylcholinesterases (AChEs), L-amino acid oxidases, nucleotidases (5′-nucleotidases, ATPases, phosphodiesterases and DNases) and hyaluronidases. In most cases, snake venoms are the most abundant source for all these enzymes. For example, *Bungarus* venoms are rich in AChE (0.8% w/w). No other tissue or biological fluid contains comparable amounts of AChE, including electric organs from electric fishes *Torpedo* and *Electrophorus* ($< 0.05\%$ w/w). Some of these enzymes are paralogs of mammalian enzymes. For example, prothrombin activators isolated from Australian snake venoms are similar to mammalian blood coagulation factors. Group D prothrombin activators are similar to factor Xa (FXa), whereas group C prothrombin activators are similar to FXa-FVa complex. Snake venom enzymes are also catalytically more active than their counterparts. In general they are more heat stable and more resistant to proteolysis due to the presence of additional disulfide bridges. Some of these enzymes exhibit exquisite substrate specificity, while others are more promiscuous. To top it off, some of them have unusual properties. For example, L-amino acid oxidase is inactivated when stored in a frozen state and is completely reactivated by heating at pH 5. High abundance and better stability (lack of

too many flexible segments) have provided impetus for structural biologists to examine the three-dimensional structures of these enzymes. In this review, we present the salient features of the major classes of snake venom enzymes, their structures, mechanisms of action and functions. When appropriate, we also discuss the inhibition of the enzymes by synthetic and natural inhibitors.

Acetylcholinesterase

Acetylcholine (ACh) is the first chemical agent known to establish a communication link between two distinct mammalian cells, and acts by propagating an electrical stimulus across the synaptic junction. AChE (EC 3.1.1.7) is a member of the cholinesterase family [3] and plays a vital role in ACh transmission in the nervous system by ensuring the hydrolysis of ACh to choline and an acetate group, thereby terminating the chemical impulse. The transmission of a chemical impulse takes place within 1 ms and demands precise integration of the structural and functional components at the synapse [4]. Incidentally, AChE may also be one of the fastest enzymes known, hydrolyzing ACh at a rate that is close to the diffusion-controlled rate [5]. The estimated turnover values of the enzyme range are approximately 7.4×10^5 to 3×10^7 ACh molecules per minute per molecule of enzyme [6,7]. The rapid hydrolysis of ACh forms the basis of rapid, repetitive responses at the synapse.

AChEs derived from vertebrates have been classified based on several criteria; the nomenclature by Bon *et al.* [8] is based on the quaternary structure and the number of glycoproteic catalytic subunits of similar catalytic activity: globular forms are named G1, G2 and G4 and contain one, two or four catalytic subunits respectively, whereas asymmetric forms are named A4, A8 and A12 and are characterized by the presence of a collagen-like tail associated with one, two or three tetramers [4,8]. In addition, depending on the presence of a hydrophobic domain responsible for anchoring the enzyme in membranes, globular forms of AChE may be further distinguished as amphiphilic and non-amphiphilic globular forms [4]. Nonetheless, all vertebrate AChEs are encoded by a single gene and the various molecular forms are generated by mRNA alternative splicing and post-translational modifications [3]. A further distinction between vertebrate AChEs is the alternatively spliced sequences which encode distinct C-terminal regions, characterizing R (read-through), H (hydrophobic), T (tailed) and, more recently, S (soluble) domains [9,10].

Outside of the cholinergic systems, the presence of AChE in cobra venom was first reported in 1938 [11]. Significant amounts of AChE are found in the venom of snakes, particularly in species belonging to the family Elapidae, with the exception of *Dendroaspis* species [12]. In contrast, AChE is not found in venoms of snakes belonging to the Viperidae and Crotalidae families [3,13]. Incidentally, snake venom AChEs are also more active than *Torpedo* and mammalian AChEs in hydrolyzing ACh [14]. However, the role of AChE in venom is enigmatic, considering that it is neither toxic nor complements other poisonous components of the venom [15].

Structure of venom AChE

Structurally, AChE purified from the venom of *Bungarus fasciatus* and other Elapidae venom exists as soluble monomers that are not associated with either anchoring proteins or cell membranes [15]. Sequence comparisons of snake venom AChE with other AChEs demonstrate that the catalytic domains of the enzymes exhibit a high level of homology. The catalytic domain of *B. fasciatus* AChE shares more than 60% identity and 80% similarity with that of *Torpedo* AChE [16]. All six cysteines, four glycosylation sites and the catalytic triad (Ser200, Glu327 and His440) are conserved in the venom AChE [16]. Similarly, 13 out of the 14 aromatic residues lining the active site cleft of the AChE including the tryptophan residue binding to the quaternary ammonium group of ACh are conserved. The principal differences between the structure of *Bungarus* AChE and *Torpedo*

AChE are the replacement of Tyr70 and Asp285 by methionine and lysine residues respectively [16,17] (Fig. 1). Tyr70 is located at the entrance to the active site cleft of *Torpedo* AChE, and relays the interaction of peripheral site ligands with the orientation of active site residue Trp84 [18–20]. The replacement of Tyr70 by methionine and serine in venom AChEs largely influences the sensitivity of the enzyme to peripheral site ligands and inhibitors [16,21].

In contrast to the well-conserved catalytic domain, the C-terminal segment of venom AChE is drastically different from mammalian AChE. The cholinesterase genes examined so far have exhibited distinct C-terminal domains [10]. *Torpedo* and mammalian AChE typically bear the R-type C-terminal domain, in which the C-terminal domain remains unspliced after the last exon coding for the catalytic domain. Invertebrate prochordates possess cholinesterase with H-type C-terminal domains that characteristically possess one or two cysteine residues near the catalytic domain, which contains a glycophosphatidylinositol anchor. The T-type C-terminal domain is observed in vertebrate AChE, and forms a hydrophobic tail that subsequently associates with other proteins or subunits to form multimers [10]. In contrast, venom AChE possesses a molecular form that is alternatively spliced from a T exon to express the S-type C-terminal domain. The S-type C-terminal domain contains a hydrophilic stretch of 15 residues consisting of six arginine and two aspartic acid residues [15,22]. The S-type domain encountered exclusively in venom AChE not only determines its classification but also determines the post-translational
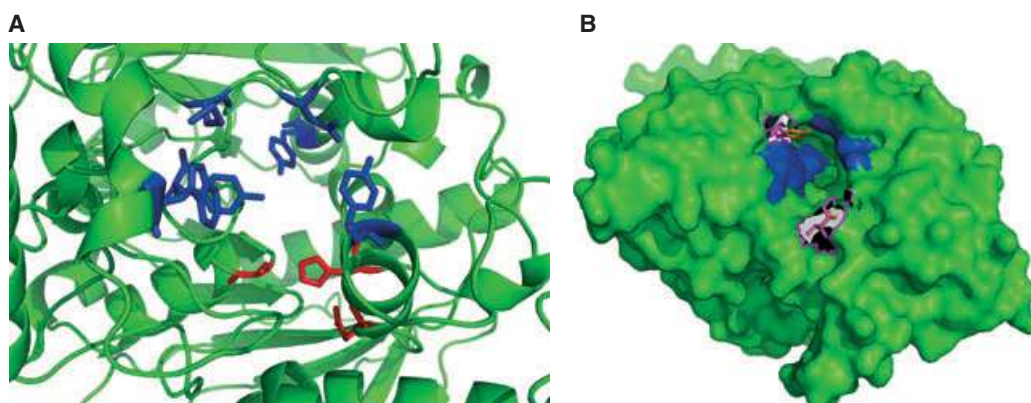
Fig. 1. Homology modeling of *Bungarus fasciatus* AChE. The structure is derived using molecular modeling with the automated mode of homology modeling on the Swiss-Model Protein Modeller Server [236–238], using *Torpedo* AChE as a template [239]. (A) The active site pocket of the modeled enzyme, with the conserved catalytic active site residues highlighted in red and the peripheral site residues highlighted in blue. (B) The entrance to the active site gorge of the enzyme, whereby Tyr70 and Asp285 (highlighted in orange) reside in close proximity to the active and peripheral site of *Torpedo* AChE. These residues are replaced by methionine and lysine residues (highlighted in magenta) respectively in the *Bungarus fasciatus* homolog.

modification (e.g. glycophosphatidylinositol anchor) and quaternary states of the AChE. More importantly, it raises important questions on the evolutionary implication of C-terminal domains in the role of AChE in neuromuscular synapses, and potentially of the role of AChE in snake venom.

Mechanism of catalysis

The structure of AChE is remarkably similar to serine hydrolases and lipases. It belongs to the α/β hydrolase family, one of the largest groups of structurally related enzymes with diverse catalytic functions. It has a β-sheet platform that bears the catalytic machinery and, in its overall features, is rather similar in all members of the family. Ser200, Glu327 and His440 residues form the catalytic triad. As in lipases and serine proteinases, glutamate residue replaces aspartate. The triad displays opposite handedness to that of serine proteinases, such as chymotrypsin, but they are in the same relative orientation in the polypeptide chain in all α/β hydrolase enzymes. The most interesting feature of AChE is the presence of a deep and narrow cleft (20 Å) which penetrates halfway into the enzyme and widens close to its base. This cleft is lined by 14 aromatic residues and it contains the catalytic triad. Two acidic residues, Asp285 and Glu273, are at the top and one, Glu199, at the bottom of the cleft. In addition, there is also a hydrogen-bonded Asp72 residue in the cleft. Rings of aromatic residues represent major elements of the anionic site of AChE, Trp84 and Phe330 contributing to the so-called catalytic anionic site (CAS), and Tyr70, Tyr121 and Trp279 to the peripheral anionic site (PAS) located on the opposite side of the gorge entrance [19]. The aromatic surface of the gorge might serve as a kind of weak affinity column down which the substrate could hop or slide towards the active site via successive π–cation interactions. AChE possesses a very large dipole moment, and the axis of the dipole moment is oriented approximately along the axis of the active site gorge. This dipole moment might serve to attract the positively charged substrate of AChE into and down the active site gorge, this being a means of overcoming the penalty of the buried active site. A potential gradient exists along the whole length of the active site gorge, which can serve to pull the substrate down the gorge once it has entered its mouth [23]. The weak hydration of ACh is thought to favor its π–cation interaction with the aromatic residues, principally Trp279 and Tyr70, at the top of the gorge, as well as subsequent interactions along the gorge towards the active site, including the two residues at the bottleneck, Tyr121 and Phe330. The strong hydration of alkali metal cations should preclude their entering the gorge due to their large diameters in their hydrated forms. Johnson *et al.* showed that the PAS traps the substrate, ACh, thus increasing the probability that it will proceed on its way to the CAS, and provided evidence for an allosteric effect of substrate bound at the PAS on the acylation step [24]. For further details on relationships between the structure and function relationships of AChE, see the review by Silman and Susssman [25].

Torpedo AChE is a classical serine hydrolase that bears a catalytic triad consisting of serine, histidine and a glutamate [17]. Consistent with the mechanism of other serine proteases, the serine residue of the catalytic triad acts as a nucleophile, while the histidine residue acts as the acid/base catalyst for the hydrolysis of the substrate (Fig. 2). For a detailed explanation of

Fig. 2. Schematic representation of *Torpedo* AChE active site. Adapted from Ahmed *et al.* [22] and Patrick *et al.* [240]. Residues involved in the catalytic triad are highlighted in red, while residues and partial contributions from the peripheral anionic sites are shaded in blue.
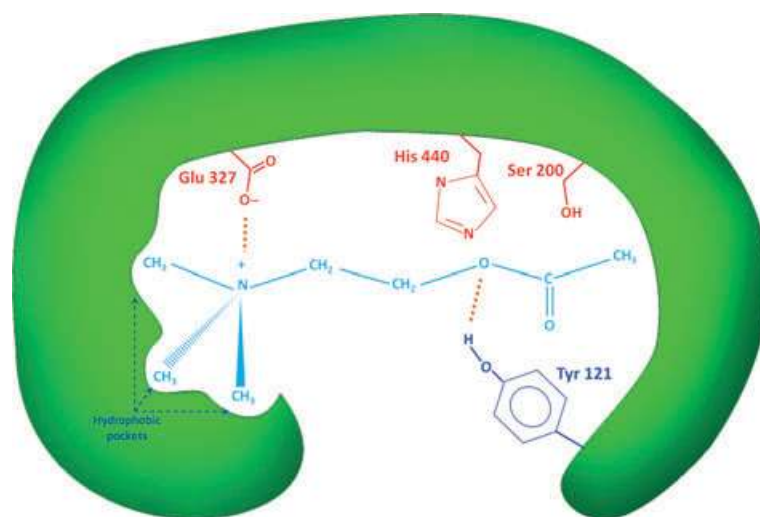
Table 1. Sensitivity of *Bungarus* AChE to inhibitory compounds [16].

Classification	Mechanism	Inhibitor	Remarks
Active site ligand	Competitive inhibitor	Edrophonium	Similar sensitivity in *Torpedo* AChE
Bis-quaternary	Mixed type inhibitor	Decamethonium	Less sensitive than *Torpedo* AChE
		BW284C51	Slightly more sensitive than *Torpedo* AChE
Peripheral site ligand	Mixed type inhibitor	Propidium	Markedly less sensitive than *Torpedo* AChE
		Gallamine	
		Fasciculin	
		D-tubocurarine	More sensitive than *Torpedo* AChE

the mechanistic steps to ACh hydrolysis by AChE, the reader is referred to the chapter by Ahmed *et al.* [22].

Effect of inhibitors

Noting the physiological significance of AChE, several inhibitors have been designed to inhibit the activity of vertebrate AChE. The effects of these inhibitors have also been studied on *B. fasciatus* AChE (Table 1). As mentioned above, both Tyr70 and Asp285 play important roles in PAS [26,27] and these residues are substituted by methionine and lysine residues respectively in *Bungarus* AChE. To understand the role of these residues on their interaction with various inhibitory ligands, the residues were reverted back in site-directed mutants (M70Y and K285D) [16]. Edrophonium is an active site ligand which competitively inhibits AChE. As expected, the M70Y and K285D mutations did not significantly alter the sensitivity of the enzyme to the inhibitor. Decamethonium and BW284C51 are bis-quaternary ligands that interact with the active site as well as the peripheral site. Both M70Y and K285D mutations increased the sensitivity to the ligands slightly, with the double mutant exhibiting a cumulative effect on the sensitivity. M70Y and K285D mutations had significant influence on the mutant *Bungarus* AChE's sensitivity to the peripheral ligands, including propidium, gallamine, tubocurarine and fasiculin. Each of the two mutations increased the enzyme's sensitivity to the inhibitors dramatically, and the cumulative effect of the two mutations was to a level that was at least as sensitive as *Torpedo* AchE [16]. These results suggest that the aromatic residue and the negative charge of the residue at positions 70 and 285 respectively in *Torpedo* AChE interact with peripheral site ligands, possibly via hydrophobic and electrostatic interactions.

L-Amino acid oxidase

L-Amino acid oxidase (LAAO, EC1.4.3.2) is a flavoenzyme catalyzing the stereospecific oxidative deamination of L-amino acids to give the corresponding α-keto acid. The enzyme has been purified from a number of different sources of snake venoms [28–32], as well as certain bacterial [33–36], fungal [37,38] and algal species [39]. The best characterized member of the family is that isolated from snake venom sources where it is found in high concentrations, constituting up to 30% of the total protein content in the venom. The enzyme from snake venom exhibits a preference for aromatic and hydrophobic amino acids such as phenylalanine and leucine.

Many of the early studies focused on the characterization of the redox and kinetic activities of *Crotalus adamantus* LAAO [40–42]. These studies showed that the enzyme goes through a ternary complex of enzyme, substrate and oxygen and that reduction of the flavin involves formation of a semiquinone [42]. As the protein is a flavoenzyme oxidase, the reduced FAD cofactor is reoxidized with dioxygen during the reductive half reaction, resulting in the formation of hydrogen peroxide.

pH- and temperature-dependent inactivation

LAAO has unusual properties; it undergoes temperature- and pH-mediated inactivation and reactivation. Wellner [43], Singer and Kearney [43a,b & c] reported heat-mediated inactivation in a pH-dependent manner. The extent of inactivation was shown to increase with pH [43], with reactivation achieved by decreasing pH and reheating the protein. Furthermore, Curti *et al.* [44] showed enzyme inactivation mediated by freezing and storage of the protein at low temperature. Freeze inactivation was most pronounced when the enzyme was stored between −20 °C and −30 °C with no inactivation apparent when stored at −60 °C. Heat-inactivated protein as well as freeze-inactivated protein was reactivated by decreasing pH and reheating the protein. Interestingly, the extent of enzyme reactivation increased at lower pH. The enzyme inactivation was accompanied by changes in spectral features and a decrease in the rate of flavin photo-mediated reduction. These results suggest that inactivation of the enzyme is due to conformational changes in the pro-
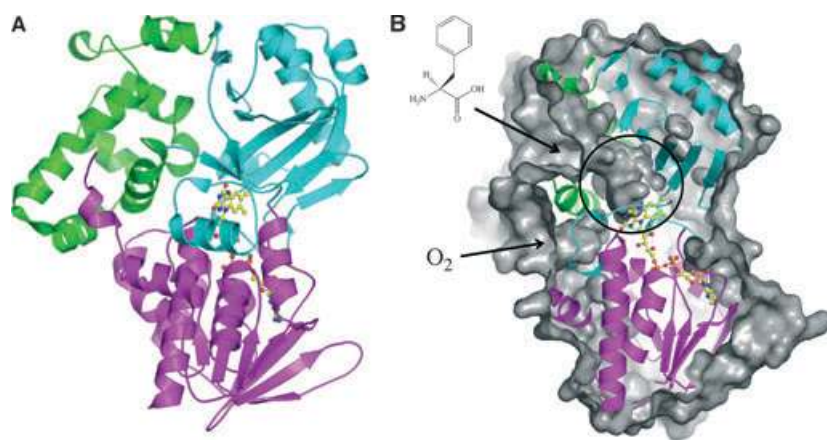
Fig. 3. The structure of L-amino acid oxidase from the snake venom of *Calloselasma rhodostoma*. (A) A ribbon representation showing the three domains of the structure: magenta coloring represents the FAD binding domain, cyan represents the substrate binding domain and green represents the helical domain. (B) The accessible surface representation of the structure: the amino acid entry and the oxygen entry points are marked with arrows and the active site is circled. The FAD molecule is shown with a ball-and-stick representation.

tein structure, particularly around the flavin binding site [44].

Structure of LAAO

Pawelek *et al.* first reported the three-dimensional structure of LAAO from the Malayan pit viper, *Calloselasma rhodostoma*, and provided important insights into the mechanism of substrate binding and catalysis by the enzyme [45]. The enzyme is composed of three domains: an FAD binding domain, a substrate binding domain and a helical domain (Fig. 3A). The FAD binding domain consists of a Rossmann fold responsible for binding the adenine, ribose and pyrophosphate moieties of the nucleotide cofactor [46,47]. Specifically, this domain contains a β–α–β motif with a consensus sequence of glycine residues ($G_{40}XG_{42}XXG_{45}$) located at the turn between the first β-strand and the α-helix. This sequence of glycine residues allows a close approach of the negatively charged phosphate moiety of the cofactor to facilitate stabilization of the charge by the helix dipole. In addition, the carboxylate side chain of a glutamate residue (Glu63) located at the carboxyl end of the second β-strand makes hydrogen bond interactions with the 2′ and 3′ hydroxyl groups of the ribose cofactor. These interactions act to bind the cofactor to the protein tightly [48].

The substrate binding domain is composed primarily of a seven-stranded mixed β-pleated sheet which forms the roof of the amino acid substrate binding pocket. Finally a helical domain, consisting of amino acid residues 130–230, contributes to a funnel-shaped entrance to the enzyme active site. The active site of the enzyme is located in a pocket deeply buried in the core of the protein located near to the isoalloxazine moiety of the flavin cofactor. Structures of enzyme complexed with the inhibitor, *o*-aminobenzoate [45], and L-phenylala-

nine [49] provided insight into the mode of substrate binding and the possible mechanism of catalysis: the carboxyl group of the amino acid substrate makes hydrogen bond contacts with the guanidinium group of Arg90 and the substrate amino group hydrogen bonds to the main chain oxygen of Gly464. The side chain of the amino acid is accommodated in a sub-pocket extending away from the isoalloxazine ring system and this pocket is composed of the side chains of Ile374, His223 and Arg322.

There are two access routes to the active site (Fig. 3B). These have been proposed to function in facilitating (a) amino acid substrate entry to, and (b) oxygen entry and peroxide release from, the buried active site. The amino acid substrate access is thought to occur through a 25 Å long funnel located between the helical domain and the substrate binding domain. The alignment of the electrostatics of the funnel to those of two bound *o*-aminobenzoate molecules found within the funnel suggests a trajectory for the substrate to take upon binding to the enzyme [45]. A second channel, narrow and hydrophobic in nature, is seen in the structure of the enzyme bound with L-phenylalanine [49]. This channel is thought to act as a conduit for O_2 access to and H_2O_2 release from the buried active site pocket.

Stereospecificity of LAAO

The structure of LAAO allowed a detailed investigation of the enantiomeric substrate specificity exhibited by the enzyme compared with D-amino acid oxidase (DAAO). Unlike LAAO, DAAO lacks the helical domain present in LAAO [50]. Furthermore, the arrangement of residues in the active sites differs between the two enzymes. Not surprisingly, stereospecificity of the two enzymes for their respective substrate

is strong; oxidation of the opposite enantiomer does not occur for either enzyme. Despite the lack of significant sequence homology between the two enzymes, a comparison of the structures showed homology in the FAD binding domain as well as similarities in the secondary structure units of the substrate binding domain. Interestingly, when a mirror image of the structure of DAAO bound to *o*-aminobenzoate was computationally constructed and superposed onto the LAAO–*o*-aminobenzoate complex, a structural conservation of amino acid residues proposed to be involved in substrate binding was observed. In addition, the alpha carbon atom of the ligand and the N5 of FAD are positioned on the mirror plane, suggesting that a 'catalytic axis' of oxidation is conserved between the two enzymes whereas divergence has occurred in order to build enantiomeric binding specificity [45].

Other LAAO structures

In addition to the structure of *Calloselasma rhodostoma* LAAO, crystal structures have also been determined of the enzymes from the venom of *Agkistrodon halys pallas* [51] and from bacterial sources including *Rhodococcus opacus* [52] and *Streptomyces* species [34], where the enzyme has been called L-glutamate oxidase, and *Pseudomonas* species, where the enzyme has been called L-phenylalanine oxidase [53]. The structures of snake venom LAAOs, L-glutamate oxidase from *Streptomyces* and L-phenylalanine oxidase from *Pseudomonas* strategically position the helical domains to seal off the active site from the external aqueous environment forming a funnel that has been proposed for substrate entry. The sequestered active site is likely to be more favorable for redox catalysis, as it creates an environment more amenable to substrate oxidation. In contrast, in the enzyme from *R. opacus*, the helical domain swings away from the active site and makes extensive contacts with the same domain in the second monomer such that an intermolecular four-helix bundle is formed. Faust *et al.* [52] have proposed that the helical domain in the *Rhodococcus* enzyme is important for dimerization. However, one cannot eliminate the possibility that different orientations of this domain may also be needed for different stages of catalysis.

Mechanism of catalysis

The structure of the enzyme in the presence of an amino acid substrate has provided insights into the mechanism of flavin-mediated substrate oxidation [49,52]. To obtain this complex, oxidized crystals of the enzyme were exposed to solutions containing L-phenylalanine or L-alanine. In the case of the snake venom enzyme, the structure also reveals significant dynamic movement of specific amino acid residues in the active site. A histidine (His223) has been proposed to act as the catalytic base for abstraction of the α-amino proton during substrate oxidation. Inspection of the level of conservation of this residue shows that it is structurally conserved in all the enzymes from snake venom. However, in the cases of the enzymes from bacterial sources, this residue is not conserved. This may suggest that either this histidine is not necessary for catalysis or that the catalytic mechanism of oxidation by the venom enzyme differs from that by the bacterial enzymes. These studies remain to be pursued.

Toxicity of LAAO

A number of studies have indicated that LAAO contributes a role to the toxicity of the venom. However, there is not a clear consensus on the mechanism of this role. Although some reports suggest that the enzyme inhibits platelet aggregation [54–56], others report that platelet aggregation is induced by the enzyme and that antibacterial effects are observed through the production of H_2O_2 [57–59]. In the early 1990s, studies by several groups showed that snake venom induced apoptotic activity in vascular endothelial cells [60–62]. The apoptotic activity is most likely related to an increase in the concentration of H_2O_2. Torii *et al.* [62] reported complete inhibition of apoptosis upon incubation of cells with catalase, a scavenger of H_2O_2. However, a number of other studies showed that cell viability was not completely recoverable in the presence of catalase, suggesting that the apoptotic effect of LAAO is not solely due to the production of H_2O_2 [61,63,64]. Studies by Ande *et al.* [63] show that apoptotic activity may be partially due to the depletion of essential amino acids from the cell.

Role of glycosylation in the toxicity of LAAO

Another factor thought to play a role in the cell death process is the presence of the glycan moiety on the enzyme, which may interact with structures at the cell surface [61,63,65]. Fluorescence microscopy using LAAO conjugated with a fluorescence label revealed a direct attachment of the protein to the cell surface of mouse lymphocytic leukemia cells [61], human umbilical vein endothelial cells, human promyelocytic leukemia cells, human ovarian carcinoma cells and mouse

endothelial cells [62] but not to human epitheloid carcinoma cells [61]. The differing levels of cytotoxic effects of the enzyme on the different cell lines suggest varying extents of cell–surface interaction between the cells and the enzyme.

The localization of the enzyme at the cell surface has been implicated in producing high concentrations of H_2O_2 localized at the membrane and attributed to apoptotic activity. The structure of LAAO from snake venom revealed electron density consistent with a carbohydrate moiety attached to the side chains of Asn172 and Asn361. Electron density for the more distal carbohydrate units was not of adequate quality to enable their identification, most probably due to the flexible nature of the glycan chain [45]. Subsequent studies using two-dimensional NMR spectroscopy and MALDI-TOF mass spectrometry on the isolated glycan enabled identification of the oligosaccharide moiety as a bis-sialylated, biantennary, core-fucosylated dodecasaccharide [66]. The glycan moiety at Asn172 lies near to the proposed O_2 entry and H_2O_2 exit channel. The co-localization of the enzyme's host-interacting glycan moiety with the H_2O_2 release site on the enzyme has been suggested as a possible mechanism for facilitating apoptosis activity. However, the full role of the glycan moiety requires further investigation.

Phospholipases A$_2$

PLA$_2$s (phosphatide 2-acylhydrolase, EC 3.1.14) represent a superfamily of lipolytic enzymes which specifically catalyze the hydrolysis of the ester bond at the *sn*-2 position of glycerophospholipids resulting in the generation of fatty acid (arachidonate) and lysophospholipids [67–70]. The PLA$_2$ superfamily consists of about 15 groups which are further subdivided into several subgroups, all of which display differences in terms of their structural and functional specificities [71,72]. However, the four main types or classes of PLA$_2$s are the secreted (sPLA$_2$s), the cytosolic (cPLA$_2$s), the Ca^{2+}-independent (iPLA$_2$s) and the lipoprotein-associated (LpPLA$_2$s) phospholipases A$_2$ [71].

The sPLA$_2$s, which were the first PLA$_2$s to be discovered, are 14–18 kDa secreted proteins and are mainly found in snake, bee, scorpion or wasp venoms [73–79], mammalian tissues such as pancreas and kidneys [80,81] and arthritic synovial fluids [82,83]. They usually contain five to eight disulfide bonds and, in order to function, these proteins need the availability of Ca^{2+} ion for the hydrolysis of phospholipids. The sPLA$_2$s from various sources belong to one of the several characteristic groups such as IA, IB, IIA, IIB,

IIC, IID, IIE, IIF, III, V, IX, X, XIA, XIB, XII, XIII and XIV [71,72]. Many of the sPLA$_2$s display the phenomenon called interfacial activation [84,85] where they demonstrate a remarkable augmentation in their catalytic activity when the substrate is presented as a large lipid aggregate rather than a monomeric form [86,87]. Initially, snake venom PLA$_2$s were classified into two groups, I and II, which are easily distinguishable based on the positions of cysteine residues in their sequences [73] (Fig. S1). The amino acid sequences show that group II PLA$_2$s have five to seven residues more than group I PLA$_2$s. There are deletions around residue 60 in group II corresponding to the elapid loop found in group I PLA$_2$s. To date crystal structures of several groups I and II PLA$_2$s have been determined both in unbound and ligand bound states [88–104]. Both types of PLA$_2$s share a homologous core of invariant tertiary structure. Since the secretory group II PLA$_2$s are considered to be important drug targets for aiding the development of new anti-inflammatory agents, they have been most extensively studied, and we shall focus here on group II secretory PLA$_2$s and their inhibition by natural and synthetic inhibitors. However, the structural details of group I PLA$_2$s are also described below.

Structure of group I secretory PLA$_2$

Group I contains mammalian pancreatic PLA$_2$s and venoms of snakes belonging to the families Elapinae and Hydrophinae. These PLA$_2$s possess seven disulfide linkages with a unique disulfide bridge formed between half cysteines 11 and 72. The six remaining disulfide bonds are Cys27-Cys119, Cys29-Cys45, Cys44-Cys100, Cys51-Cys93, Cys61-Cys86 and Cys79-Cys91 (sequence numbering has been indicated in Fig. S2).

To date, crystal structures of several group I PLA$_2$s are known [94,96,100,101,104,105]. The structures consist of an N-terminal helix H1 (residues 2–12), helix H2 (residues 40–55) and helix H3 (residues 86–103). There are other two short 3_{10} helices involving residues 19–22 (SH4) and 108–110 (SH5) (Fig. S2). They also contain a β-wing with two short antiparallel β-strands, 70–74 and 76–79. The presence of calcium ion in the structure is stabilized by sevenfold pentagonal coordination: two carboxylate oxygen atoms of Asp49, three main chain oxygen atoms of Tyr28, Gly30 and Gly32, and two oxygen atoms of two structurally conserved water molecules. The ligand binding site in group I PLA$_2$ consists of residues Leu2, Phe5, Ile9, Trp19, Phe22, Ala23, Gly30 and Tyr64. The wall at the back of the protein molecule contains active site residues His48, Asp49, Tyr52 and Asp94.
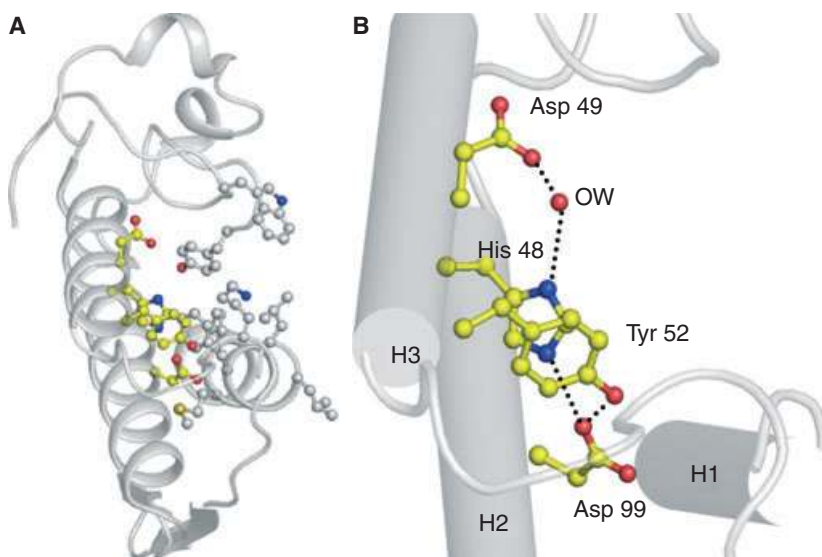
Fig. 4. The three-dimensional structure of PLA$_2$. (A) A view of the PLA$_2$ structure showing active site residues in yellow. The substrate diffusion channel with hydrophobic residues Leu2, Leu3, Phe5, Ile9, Tyr22, Trp31 and Lys69 is also seen. (B) The catalytic network in PLA$_2$ is shown. OW indicates a water molecule oxygen atom which serves as the nucleophile. The dotted lines indicate hydrogen bonds.

Structure of group II secretory PLA$_2$

Group IIA along with groups V and X sPLA$_2$s are highly expressed in humans and mouse atherosclerotic lesions where each group contributes differentially to atherogenesis [106,107]. All three sPLA$_2$s are relevant for drug design, but group IIA PLA$_2$ has been investigated the most extensively (Fig. S3).

The crystal structures of a large number of isoforms of group IIA PLA$_2$ are already available [92,93,95,97–99,102,104,108,109]. There are three main α-helices: N-terminal helix H1 (residues 2–12), helix H2 (residues 40–55) and helix H3 (residues 90–108). The α-helices H2 and H3 are antiparallel and are at the core of the protein. There are two additional short helices SH4 (residues 114–117) and SH5 (residues 121–125), as well as a short two-stranded (residues 74–78 and 81–84) antiparallel β-sheet which is called the β-wing. There are two functionally relevant loops, the calcium binding loop (residues 25–35) and a very characteristic and flexible external loop (residues 14–23).

The α-helices H2 and H3 are amphipathic in nature with their hydrophilic side chains exposed to the solvent and the hydrophobic side chains buried deep inside the protein interior with the only notable exceptions being the four highly conserved residues in the active site: His48, Asp49, Tyr52 and Asp99. A significant structural feature of the activation domain of the PLA$_2$ molecule is the hydrophobic channel which begins from the surface and spans across the width of the molecule diagonally and widens to be finally connected to the active site. The entrance of this channel is flanked by the bulky side chains of Trp31 and Lys69. The walls of this channel are lined up by several hydrophobic residues including Leu2, Phe5, Met8, Ile9, Tyr22, Cys29, Cys45, Tyr52, Lys69 Ala102, Ala103 and Phe106 (Fig. 4A).

The active site of the PLA$_2$ molecule is a semicircular cavity at the end of the hydrophobic channel. It consists of four residues: His48, Asp49, Tyr52 and Asp99. A conserved water molecule plays an essential role in the catalysis and is connected to the side chains of the active site residues His48 and Asp49 through hydrogen bonds (Fig. 4B). Based on the extensive structural data of PLA$_2$s in their native states [91–93,109] and in complexes with small molecules [88,90,91,93,110–118], six distinct subsites have been defined in the PLA$_2$ enzyme, namely subsite 1 (residues 2–10), subsite 2 (residues 17–23), subsite 3 (residues 28–32), subsite 4 (residues 48–52), subsite 5 (residues 68–70) and subsite 6 (residues 98–106) (Fig. S4).

Mechanism of action

Catalytic action

The catalytic network in secretory PLA$_2$ resembles those of serine proteinases [75,119,120]. The reaction mechanism follows a general base-mediated attack on the sessile bond through the involvement of a conserved water molecule which serves as a nucleophile. The residues involved in catalysis and their hydrogen bonding network are illustrated in Fig. S5.

Interactions of PLA$_2$ with substrate analogs

The interactions of the substrate analogs provide valuable information about the potential recognition ele-
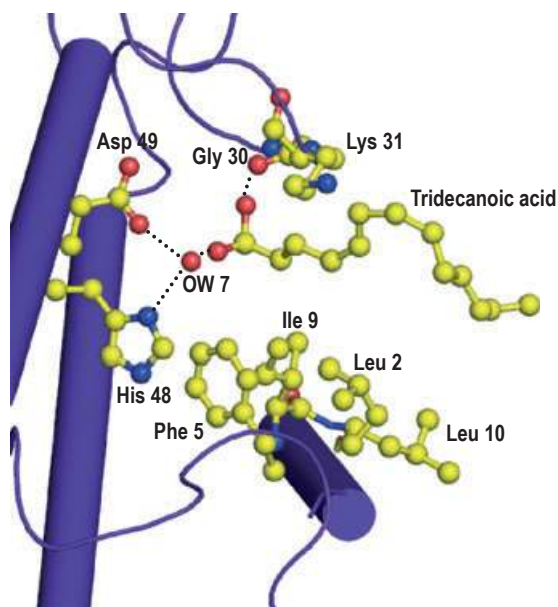
Fig. 5. Interactions of PLA$_2$ with a substrate analog tridecanoic acid. The dotted lines indicate hydrogen bonds.

ments in the substrate binding site. Therefore, the complex of PLA$_2$ with tridecanoic acid was examined (Fig. 5). One of the carboxylic group oxygen atoms of tridecanoic acid forms a hydrogen bond with the conserved water molecule designated as OW while the second oxygen atom forms another hydrogen bond with Gly30 N. The hydrocarbon chain of tridecanoic acid is placed in such a way as to form a number of van der Waals contacts Leu2, Leu5, Met8 and Ile9 of the hydrophobic channel.

Inhibition of PLA$_2$

The binding affinities of all known ligands of PLA$_2$ are in the range 10^{-4}–10^{-8} M, which make them poor to moderate candidates as drugs. Examination of the structures PLA$_2$ complexed with the known ligands showed that the poor potency can be attributed to the fact that these compounds are able to occupy only a few of the subsites within the overall substrate binding space, hence generating only a limited number of interactions with the protein. Thus, keeping the stereochemical features of the subsites in the substrate binding site in mind, there is an immense possibility to design highly potent inhibitors.

Inhibition of PLA$_2$ by natural compounds

Although there have been numerous reports on natural compounds inhibiting PLA$_2$, only five crystal struc-

tures of complexes of PLA$_2$ with natural compounds have been reported [91,93,101,116]. These compounds include aristolochic acid, vitamin E and atropine (Fig. S6). All the natural compounds studied so far have been shown to fit in the active site with the classical 'head to tail' hydrogen bonded interactions between the hydroxyl groups or oxygen atoms of the ligand with the active site residues of PLA$_2$ molecule, in which His48 and Asp49 form hydrogen bonds either directly or through the conserved water molecule that bridges His48 and Asp49. They bind to PLA$_2$ in a similar manner at the substrate binding site but occupy the subsites according to the size of their hydrophobic moiety. As a result, these compounds are similarly placed in the hydrophobic channel. While subsites near the active site residues are similarly saturated, subsites distant from the active sites are dissimilarly occupied.

The hydroxyl groups of both aristolochic acid and vitamin E form two hydrogen bonds with the side chains of His48 and Asp49. The conserved water molecule in both these cases has been replaced by the hydroxyl moieties of these compounds and generates direct hydrogen bonding interactions. In the case of atropine, while the oxygen atom of the atropine makes a direct hydrogen bond with His48, it also makes indirect interactions with the active site residues His48 and Asp49 through the conserved water molecule. Additionally, the hydroxyl group of atropine forms a hydrogen bond with the carbonyl group of Asp49. Unlike that of vitamin E and aristolochic acid, the conserved water molecule in the active site of the PLA$_2$ is not displaced by atropine.

Inhibition of PLA$_2$ by indole compounds

In recent years, there have been several reports on the inhibition of secretory PLA$_2$ by indole derivatives, notably complexes of human secretory PLA$_2$ with indolizine inhibitors [113], human non-pancreatic secretory PLA$_2$ with indole inhibitors Indole-3 [(1-benzyl-5-methoxy-2-methyl-1H-indol-3-yl)-acetic acid], Indole-6 [4-(1-benzyl-3-carbamoylmethyl-2-methyl-1H-indol-5-yloxy)-butyric acid] and Indole-8 [{3-(1-benzyl-3-carbamoylmethyl-2-methyl-1H-indol-5-yloxy)-propyl}-phosphonic acid] [114], and complex of PLA$_2$ with the indole derivative [2-carbamoyl methyl-5-propyl-octahydroindol-7-yl-acetic] acid [88]. Additionally, there is a molecular modeling study which highlights the importance of various substitutions of indole derivatives and resulting interactions with PLA$_2$ [121].

In all the crystal structures of the complexes of PLA$_2$ with the indole derivatives, the indole molecule is positioned in the hydrophobic channel and makes

hydrogen bonds with His48 and Asp49 through its ethanamide group, mimicking the nature of inhibition of natural compounds, by displacing the conserved catalytic water molecule in the active site of the molecule. The ethanamide group appears to be more preferred than the hydroxyl group for intermolecular interactions involving Asp49 and His48 of the catalytic network in PLA$_2$. Upon comparison of this structure with the other complexes of human PLA$_2$ with indole derivates [114], it was observed that essentially all the indole molecules and their derivatives occupied the same binding site in the hydrophobic channel of PLA$_2$ (Fig. S7). It is noteworthy that the orientations of the indole ring of various derivatives in the hydrophobic channel remain unaltered which indicates a degree of complementarity of indole derivatives *vis-à-vis* the hydrophobic channel in PLA$_2$. It has been indicated that the substitutions at different sites of indole rings alter the binding constants [122]. Accordingly, the complexes show different binding interactions and hence different affinities.

Inhibition of PLA$_2$ by NSAIDs

The structure analyses of the complexes with non-steroidal anti-inflammatory drugs (NSAIDs) was carried out primarily for understanding the mechanisms of action of NSAIDs [117,118,123] and they led to several interesting and yet unpredictable observations. It was observed that most of the NSAIDs bind to PLA$_2$ in the conventional manner (Fig. S8A,B); they bind either directly with the help of interactions with His48 and Asp49 or indirectly through the conserved water molecule. Indomethacin, one of the most potent NSAIDs, was found to be interacting with PLA$_2$ in a different mode: one of the carboxylic group oxygen atoms forms a hydrogen bond with the catalytic water molecule while the second oxygen atom interacts with Lys69 (Fig. S8C).

Inhibition of PLA$_2$ by designed peptides

The atomic details of PLA$_2$ have been structurally analyzed and the results have revealed useful details of the hydrophobic channel leading to the active site. To harness the structural knowledge of PLA$_2$ ligand binding site for drug design, highly specific peptide inhibitors of PLA$_2$ showing binding affinities at 10^{-9} M concentrations were designed, synthesized and co-crystallized with PLA$_2$.

A peptide with the sequence Leu-Ala-Ile-Tyr-Ser (LAIYS) was designed with hydroxyl moiety containing residues tyrosine and serine at the carboxyl terminus that can make hydrogen bonds with His48 and Asp49 and the Leu-Ala-Ile moiety for generating hydrophobic interactions with the protein residues lined up along the hydrophobic channel. The structure analysis of the complex of LAIYS with PLA$_2$ revealed that the inhibitor occupied the substrate binding site in a tight fit. As predicted, the hydroxyl group of the side chain of tyrosine was found to be interacting with Asp49 and His48 while the hydrophobic residues of the peptide were involved in the interactions with the residues of the hydrophobic channel (Fig. 6A). The close fit of the peptide was substantiated with the high binding affinity of $\sim 8.8 \times 10^{-9}$ M estimated using surface plasmon resonance experiments. In a further attempt to exploit the negative charge on Asp49 and the positive charge on His48, a peptide Phe-Leu-Ser-Tyr-Lys (FLSYK) with a lysine residue at the C-terminus was designed. The structure of the PLA$_2$ complex with peptide FLSYK revealed that the side chain of lysine was well placed in the active site and its NH$_2$ group made a strong ionic interaction with the side chain of Asp49 while the negatively charged carboxyl group of the peptide interacted with His48 (Fig. 6B). Predictably, due to stronger ionic interactions, the peptide FLSYK displayed a high binding affinity of 1.1×10^{-9} M.
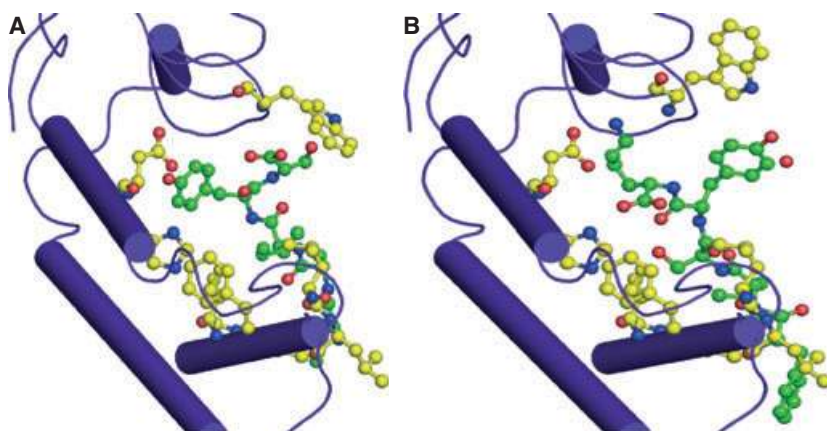
Fig. 6. Structures of two representative PLA$_2$ complexes with designed peptides: (A) Leu-Ala-Ile-Tyr-Ser (LAIYS) and (B) Phe-Leu-Ser-Tyr-Lys (FLSYK). The interactions with peptide LAIYS involve the hydroxyl group of peptide tyrosine that forms two hydrogen bonds with protein residues His48 and Asp49. The interactions with peptide FLSYK include two important ionic interactions involving the side chains of Lys and Asp49 while the C-terminal carboxyl group of peptide interacts with the side chain of His48 of the protein.
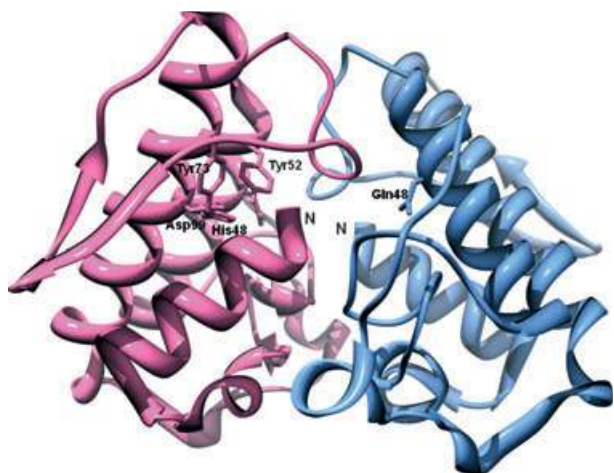
Fig. 7. The structure of vipoxin (PDB code 1JLT). The basic, toxic and catalytically active subunit is colored in red. The active site residues are shown. The acidic and non-toxic subunit is colored in blue. The substitution in position 48 in the acidic chain is also shown.

Overview of inhibitor design

The analysis of interactions of PLA_2 with various ligands including the designed peptides reveals that the ligands containing OH or COOH groups interact directly with the side chains of active site residues His48 and Asp49. The presence of carbonyl or carboxyl groups in ligands tends to promote interactions with protein through conserved water molecules. The peptides containing residues with side chains of serine, threonine or tyrosine interact directly with His48 and Asp49 through bifurcated hydrogen bonds. However, peptides containing positively charged side chains of Lys or Arg at the C-terminus form ionic interactions through their side chains with Asp49 while the carboxyl terminal of the peptide forms ionic interactions with the side chain of His48. Additional hydrogen bonds have been observed involving Gly30 NH and Trp31 $N^{\varepsilon 1}$. The hydrophobic moieties of ligands and peptides form interactions with protein residues Leu2, Leu3, Phe5, Ile9, Leu10, Ala18, Ile19, Phe22, Ala23, Tyr28, Gly30, Trp31, Gly32, Tyr52, Tyr63, Tyr64, Lys69, Phe98, Phe101 and Phe106.

Heterodimeric neurotoxic PLA_2 complexes

In venoms, PLA_2s function as monomers or multimeric complexes in which at least one subunit is catalytically active. Non-covalent heterodimeric PLA_2 complexes (ncHdPLA$_2$s) are neurotoxins with a sophisticated mechanism of action in comparison with their monomeric counterparts. ncHdPLA$_2$s were isolated from Crotalinae and Viperinae snakes. They consist of a basic toxic PLA_2 and an acidic non-toxic and enzymatically inactive PLA_2-like protein which probably results from accelerated evolution for acquisition of diverse physiological function. The acidic subunits are multifunctional and differ in their function: in addition to targeting the toxic component to specific membrane receptors, they potentiate or inhibit the PLA_2 toxicity and, in some cases, can modulate its catalytic activity and stabilize the other subunit. ncHdPLA$_2$s differ mainly in the structure of the acidic subunit. Comparison of ncHdPLA$_2$s from snakes inhabiting South America, Europe and Asia showed unexpected structural identity. We describe and discuss structure–function relationships of ncHdPLA$_2$s using mainly crystallographic investigations and results on the heterodimeric neurotoxins and their components.

Structural investigations on crotoxin

The Crotalinae subfamily consists of over 190 species in 29 genera [124] found in the Americas and Asia. These are the only viperids found in the Americas. A heterodimeric neurotoxin was isolated for the first time in 1938 by Slotta and Fraenkel-Conrat from the venom of the south American rattlesnake *Crotalus durissus terrificus* and called crotoxin [125]. It consists of a basic PLA_2 with low toxicity subunit B or crotactin and an acidic, non-toxic polypeptide, subunit A or crotapotin. The second subunit has no enzymatic activity and consists of three polypeptides linked by disulfide bonds [126]. Crotoxin was identified as a presynaptic toxin. The crotoxin subunits dissociate in the presence of synaptic membranes [127]. The acidic component of the neurotoxic complex increases the lethal potency of the crotoxin basic PLA_2 [128]. In this respect it differs from the acidic subunit of vipoxin, another ncHdPLA$_2$ from the venom of the European snake *Vipera ammodytes meridionalis*, which reduces the neurotoxicity of the basic component [129]. At least 15 homologous isotoxins have been isolated so far [130]. A single *Crotalus d. terrificus* snake produces up to 10 different crotoxin-like toxins [130]. The three-dimensional structure of this toxin complex is not yet known. The heterodimer and its isolated subunits were crystallized and preliminary X-ray data were collected [131]. The structure of crotapotin was studied by small-angle X-ray scattering [132]. Recently, the structure of a tetrameric complex of the crotoxin basic subunit B was reported [133].

Crotoxin-like neurotoxin complexes have been identified from the venom of other rattlesnake species,

including *Sistrurus catenatus tergeminus*, *Crotalus mitchelli mitchelli*, *Crotalus horridus atricaudatus*, *Crotalus basiliscus* and *Crotalus durissus cumanensis* [134]. Among these crotoxin-like complexes, the ncHdPLA$_2$ complex Mojave toxin isolated from the venom of *Crotalus scutulatus scutulatus* is one of the best characterized, and is structurally and functionally similar to crotoxin [135].

Structural investigations on vipoxin

The venomous viper species *Vipera ammodytes* of the subfamily Viperinae is the most dangerous of the European vipers [136]. Vipoxin, a neurotoxic ncHd-PLA$_2$, represents the first ncHdPLA$_2$ isolated from the venom of a European venomous snake, in this case *Vipera a. meridionalis* [137]. Vipoxin is composed of a basic, highly toxic group IIA PLA$_2$ and a non-toxic catalytically inactive PLA$_2$-like protein [138]. Vipoxin is unusual; it has an acidic subunit (Inh) which inhibits the catalytic activity of the basic component up to 60% and decreases considerably (fivefold) its toxicity [129]. The two subunits are closely related proteins, with 62% sequence identity [139]. However, due to the substitution of the active site His48 by glutamine, Inh has no enzymatic activity. Vipoxin is a postsynaptic neurotoxin, but the separated basic PLA$_2$ acts at presynaptic level changing the target of the physiological attack [138]. The acidic component of vipoxin is a natural inhibitor of the basic and catalytically active PLA$_2$. In the absence of the PLA$_2$-like protein, the toxic component loses its catalytic activity after 2 weeks at 0 °C and the toxicity gradually decreases [129]. In the presence of the acidic subunit the toxin is stable for years. Most probably, Inh is a product of divergent evolution in order to stabilize the relatively unstable PLA$_2$ and to preserve the pharmacological activity of the toxin for a long period. Vipoxin is the first reported example of a PLA$_2$ acquiring an inhibitory function [140].

We analyzed the vipoxin structure at 1.4 Å resolution [108]. The three-dimensional structures of the two subunits are identical (Figure 7) which confirms the hypothesis that the enzymatically non-active and non-toxic acidic component of the complex, modulating both the enzymatic activity and toxicity of the basic subunit, is a product of divergent evolution of the catalytically active and toxic PLA$_2$. The salt bridge between Asp48 of the PLA$_2$ molecule and Lys60 of the acidic subunit (Asp49 and Lys69 according to the numbering of Renetseder *et al.* [141]) stabilizes the whole complex. The X-ray model revealed that hydrophobic forces and electrostatic interactions between the

two oppositely charged subunits provide further stability to the heterodimer. In this way the toxic subunit preserves the catalytically and physiologically active conformation. The acidic subunit partially shields the entrance to the active site of PLA$_2$ but this does not preclude the access of small substrates. Only the reaction velocity is decreased which explains the reduced enzymatic activity of the basic subunit towards synthetic substrates when it is in a complex with Inh. However, in the presence of aggregated substrates the complex dissociates [142] and the liberated PLA$_2$ is fully active. The non-toxic subunit partially blocks the segment 109–114 (residues 119–125 according to Renetseder *et al.* [141]) of the PLA$_2$ important for the neurotoxicity.

Elaidoylamide is a powerful inhibitor of the vipoxin toxic PLA$_2$. The crystal structure of the vipoxin PLA$_2$–elaidoylamide complex (Fig. 8) revealed a new mechanism of inhibition: one molecule of elaidoylamide is bound simultaneously to the hydrophobic channels of the substrate binding sites of two associated PLA$_2$ molecules [143]. This observation is of pharmacological interest and can be used to support the design of new anti-inflammatory drugs.

The interaction of snake venom PLA$_2$ toxins with negatively charged surface regions is an important initial step during the catalysis. The non-catalytic subunit of vipoxin targets the toxic component to the
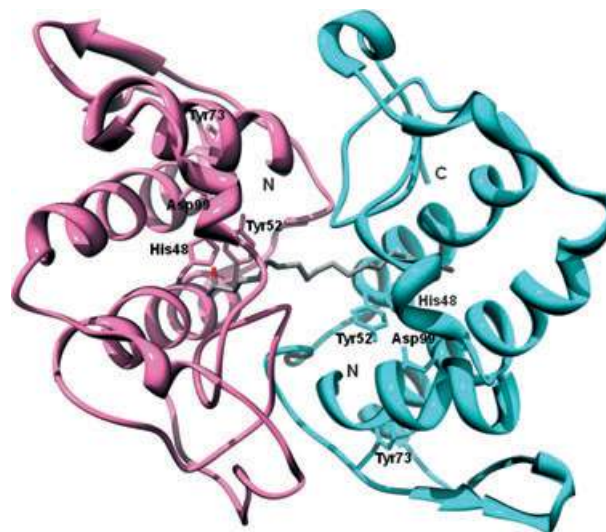
Fig. 8. The three-dimensional structure of the complex between the vipoxin toxic PLA$_2$ and elaidoylamide (PDB code 1RGB). The structure demonstrates a new mode of PLA$_2$ inhibition: one molecule of the fatty acid derivative inhibits two neurotoxic molecules blocking their substrate binding channels. The chain of the inhibitor elaidoylamide is colored in black.

negatively charged membrane surface [130,142]. We analyzed the 1.9 Å structure of the vipoxin non-toxic subunit complexed to sulfate ions which mimic negatively charged groups on anionic membranes [144]. The crystallographic model of the dimeric Gln48 PLA_2 revealed two anion binding sites per subunit. Site 1 is common for the two monomers. It is located at the C-terminus of the polypeptide chain, in a region which in the basic PLA_2 is involved in neurotoxic activity. The sites of the non-catalytic protein of the vipoxin complex may interact with negative charges on synaptic membranes.

Structural investigations on viperotoxin F

An ncHdPLA₂ presynaptic heterodimeric neurotoxin, viperotoxin F, was isolated from the venom of *Vipera russelli formosensis* (Taiwan Russell's viper) [145]. It consists of two subunits: a basic and neurotoxic PLA_2 (RV-4) and an acidic non-toxic component with a very low enzymatic activity (RV-7). RV-7 potentiates the lethal effect of RV-4 and reduces its enzymatic activity [145]. It is surprising that viperotoxin F from the Taiwan viper (Asia) is structurally closely related to vipoxin from *Vipera a. meridionalis* (southeast Europe). There are significant differences in the biochemical and pharmacological properties of the two neurotoxins: vipoxin exerts postsynaptic effects while viperotoxin F is a presynaptic toxin; the acidic component reduces the neurotoxicity of the basic PLA_2 in the first case while RV-7 potentiates the toxicity of the other subunit; RV-7 possesses low PLA_2 activity preserving the catalytically active His48 while the vipoxin acidic component has no catalytic activity due to the substitution of the active site His48 by Gln48. We have crystallized viperotoxin F and the structure was solved at 1.9 Å resolution [146]. Comparison of the vipoxin and viperotoxin F X-ray structures showed that major differences in the conformation and amino acid substitutions are located on the molecule surfaces. This is in accordance with the theory of Kini and Chan [147] that the mutational rates of the surface residues in PLA_2 enzymes are much higher than those of the buried residues.

Structural investigations on β-bungarotoxins

β-Bungarotoxin (β-BTx) is a presynaptic heterodimeric neurotoxin isolated from *Bungarus multicinctus* (Taiwan banded krait, Asia) [148]. It is a covalent complex between group I PLA_2 (chain A) and a Kunitz type serine protease inhibitor (chain B) [149]. Sixteen isoforms of the β-BTx are known [150,151]. The crystal structure of this toxin was determined at 2.45 Å resolution [152]. The structure of the enzymatically active subunit is similar to that of other class I PLA_2s. Chain B is structurally similar to the bovine pancreatic trypsin inhibitor. Interactions between the subunits in the interface region create conformational changes in both chains. The molecular recognition by the ion channel binding region of the Kunitz module differs from that of other related proteins [152].

Snake venom serine proteinases (SVSPs)

Serine proteinases catalyze the cleavage of covalent peptide bonds in proteins and play key roles in diverse biological processes ranging from digestion to the control and regulation of blood coagulation, the immune system and inflammation [153]. They probably originated as digestive enzymes and subsequently evolved by gene duplication and sequence modifications to serve additional functions [154]. They are grouped into six major clans and further subdivided into families based on sequence and functional similarities (MEROPS classification, http://merops.sanger.ac.uk; [155]): SVSPs are exclusively from clan SA and specifically belong to the S1 family. They interfere with the regulation and control of key biological reactions in the blood coagulation cascade, fibrinolytic system and blood platelet activation. Despite significant sequence identity (50–70%), SVSPs display high specificity toward distinct macromolecular substrates [156]. Based on their biological roles, they have been classified as activators of the fibrinolytic system, procoagulant, anticoagulant and platelet-aggregating enzymes [157].

The procoagulant SVSPs activate FVII [158], FX and prothrombin [159] and shorten the coagulation times. Some SVSPs also possess fibrinogen-clotting activity [160] and are often referred to as thrombin-like enzymes. Thrombin-like enzymes have been extensively investigated over the last decade for potential therapeutic uses. For example, ancrod, batroxobin and reptilase are available commercially for the treatment of cardiovascular diseases [161–163]. Ancrod is used clinically for the treatment of heparin-induced thrombocytopenia and thrombosis and acute ischemic stroke [161]. Batroxobin is used for the treatment of thrombotic diseases [162]. Batroxobin and ancrod are under clinical trials for the treatment of deep vein thrombosis. Additionally, reptilase is used as a diagnostic tool for disfibrinogenemia [163].

The anticoagulant SVSPs activate protein C via a thrombomodulin-independent mechanism [163]. The most studied SVSP enzyme is from *Agkistrodon contor-*

trix contortrix venom, commercially referred to as Pro-tac®, which specifically converts protein C to activated protein C by hydrolyzing the Arg169–Leu170 bond, functioning independently of plasmatic factors. This is in contrast to the physiological activation of protein C by thrombin, which is dependent on thrombomodulin [163]. Protac® is used clinically in functional assays of protein C determination, total protein S content, and other protein S assays in plasma [164].

Fibrinolytic SVSPs have been isolated from the venoms of *Trimeresurus stejnegeri* [165], *Agkistrodon blomhoffii* [166] and *Lachesis muta muta* [167]. These enzymes convert plasminogen to plasmin that rapidly degrades preexisting clots. The most studied fibrinolytic SVSP is the *T. stejnegeri* venom plasminogen activator (TSV-PA), which cleaves the Arg561–Val562 bond in plasminogen with high specificity and is resistant to inhibition [168].

From the above-mentioned clinical applications of SVSPs, it is clear that, in addition to their importance in snake envenomation, these venom enzymes also serve as important tools in the study of hemostasis and are clinically used for clotting assays, diagnosis, determination of protein C, protein S, plasma fibrinogen, study of platelet function, as defibrinogenating agents, to investigate desfibrinogenemias, test the contractile system of platelets, and for defibrinogenation of plasma.

Overall structure

Similar to chymotrypsin-like serine proteinases, the structures of SVSPs consist of approximately 245 amino acid residues, each containing two-six-stranded β-barrels that have evolved by gene duplication (Fig. 9A). SVSPs are unique since they possess an extended C-terminal tail, which forms an additional disulfide bridge that is considered to be important for structural stability and allosteric regulation [156] (Fig. 9B).

The N-terminal subdomain is composed of six β-strands, as well as a short α-helix positioned between strands 3 and 4 on which the catalytic residue His57 (all sequence numbering is based on chymotrypsinogen) is located. This domain is stabilized by an intra-chain disulfide bridge (Cys42/Cys58) and two other disulfide bridges (Cys22/Cys157 and Cys91/Cys245E), the latter of which is unique to SVSPs (Fig. 9B). In addition, the N-terminal subdomain contains two putative glycosylation sites positioned in the loops between strands 1 and 2, and 4 and 6 (Fig. 9B), which play a pivotal role in macromolecular selectivity of SVSPs. The catalytically important residue Asp102 is also located in this domain and precedes strand 6.
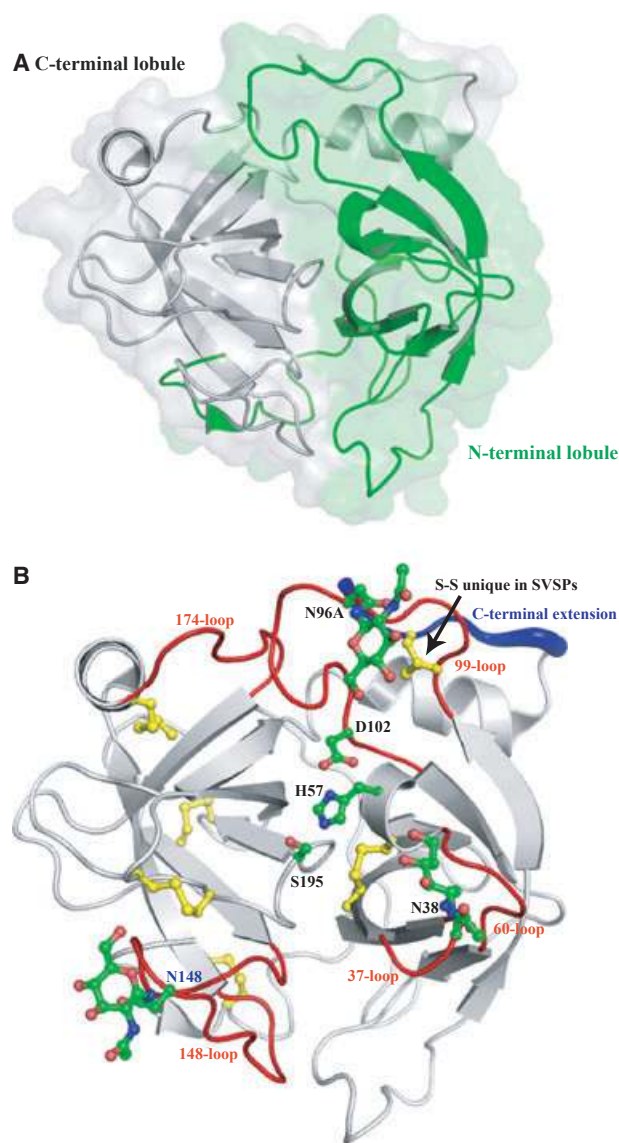
Fig. 9. The structure of SVSPs. (A) Cartoon and surface representations of SVSPs highlighting the two-six-stranded β-barrel structural lobes (in green and grey). The N-terminal domain contains six β-strands and a single short α-helix. (B) Cartoon representation of SVSPs; the extended C-terminal tail which contains an additional disulfide bridge is presented in blue. The side chains of His57, Asp102 and Ser195 are included (atom colors) as are the two putative N-linked glycosylation sites (positions N96A and N148). The intra-chain disulfide bridge Cys42/Cys58 and two other disulfide bridges Cys22/Cys157 and Cys91/Cys245E are included.

The C-terminal subdomain encompasses the six-stranded β-sheet and contains two α-helices, one inserted between strands 8 and 9, and the other located at the C-terminus preceding the extended C-terminal tail; a disulfide bridge interconnects the tail with the N-terminal subdomain (Fig. 9). This subdomain is further stabilized by three disulfide bridges Cys136/

Cys201, Cys168/Cys182 and Cys191/Cys220. The reactive serine residue at position 195 is positioned in the loop between strands 9 and 10 of this subdomain (Fig. 9B). A third glycosylation site typically encountered in SVSPs is located in the loop between strands 7 and 8 (Fig. 9B).

Active site

The catalytic triad (His57, Asp102 and Ser195) is positioned at the junction between the two barrels and is surrounded by the conserved 70-, 148- and 218-loops, as well as the non-conserved 37-, 60-, 99- and 174-loops (Fig. 9B). The catalytic residue His57 possesses a non-optimal Nδ1-H tautomeric conformation which is essential for catalysis. The catalytic triad is supported by an extensive hydrogen bonding network formed between the Nδ1-H of His57 and Oδ1 of Asp102, as well as between the OH of Ser195 and the Nε2-H of His57. The hydrogen bond between the latter pair is disrupted upon protonation of His57. Recent studies suggest that Ser214, which was once considered essential for catalysis, only plays a secondary role [169,170]. Hydrogen bonds formed between Oδ2 of Asp102 and the main chain NHs of Ala56 and His57 are structurally important to ensure the correct relative orientations of Asp102 and His57.

A salient feature of chymotrypsin-like enzymes is the presence of an oxyanion hole formed by the backbone NHs of Gly193 and Ser195. These atoms contribute to form a positively charged pocket that activates the carbonyl of the scissile peptide bond and additionally stabilizes the negatively charged oxyanion of the tetrahedral intermediate. The oxyanion hole is structurally linked to the catalytic triad and the Ile16−Asp194 salt bridge via Ser195.

Substrate recognition sites – subsites

Subsites are structural motifs involved in the recognition and binding of the substrate. Based on the nomenclature of Schechter and Berger [171], the specificity of proteases is generally focused on S1/P1 and S1′/P1′ interactions and additionally on positions S2/S2′ and S3/S3′. Specificity of chymotrypsin-like serine proteases is generally classified in terms of the P1−S1 interaction. The S1 site pocket lies adjacent to Ser195 and is formed by residues 189−192, 214−216 and 224−228. Specificity is usually determined by the residues at positions 189, 216 and 226 [172]. Chymotrypsin has a high preference for hydrophobic residues at the S1 subsite due to the deep hydrophobic pocket formed by Ser189, Gly216 and Gly226 [119]. On the other hand, the S1

subsite in trypsin-like enzymes is populated by Asp189, Gly216 and Gly226, which create a negatively charged S1 subsite that accounts for trypsin's preferred specificity for substrates containing Arg or Lys at P1 [173].

SVSPs are trypsin-like enzymes with highly conserved S1 subsites, but exhibit high selectivity towards macromolecular substrates such as blood coagulation factors [165,174]. Since catalysis and specificity are not controlled by the characteristics of a few residues but are properties of the entire protein's structural and biochemical framework, the structural basis for SVSPs' selectivity remains unclear. However, structural studies of TSV-PA [175] and Protac® [156] have suggested the importance of key specific elements that might be responsible for their high substrate selectivity.

In Protac® [156], the three carbohydrate moieties strategically positioned at the tips of the 37-, 99- and 148-loops form the entrance to the active site pocket and could play important roles in the modulation and expression of selectivity towards macromolecular substrates (Fig. 9B). Two snake venom serine proteinase isoforms from *Agkistrodon acutus*, AaV-SP-I and AaV-SP-II, also possess an N-linked carbohydrate group (Asn35) that is considered to interfere with the binding of macromolecular inhibitors [176]. Another key structural element implicated in the functional differentiation in SVSPs is the surface charge distribution. Murakami and Arni [156] suggested that the charge around the interfacial surface of Protac® mimics the thrombin–thrombomodulin complex presenting high electrostatic affinity for the Asp/Glu pro-peptide of protein C (Fig. 10).

In the case of TSV-PA, the enzyme has a unique glycosylation site at the Asn178 residue located on the opposite face and apparently does not play a role in the binding of macromolecular substrates at the interfacial site [175]. Mutational studies of TVS-PA demonstrated that Asp97 is crucial for the enzyme's plasminogenolytic activity. In addition, phylogenetic analysis demonstrated conservation of this key residue in both types of mammalian plasminogen activator (tissue type and urokinase type), thereby supporting the hypothesis that Asp97 could be a common element for plasminogen recognition [168].

Mechanism of catalysis

The first step to the highly efficient acid–base catalytic mechanism of SVSP involves Ser195, which initiates the attack on the carboxyl group of the peptide. The reaction is assisted by His57 which acts as a general base to form the tetrahedral intermediate, stabilized by interactions with the main-chain NHs of the oxyanion

Protein C activator   **Plasminogen activator**
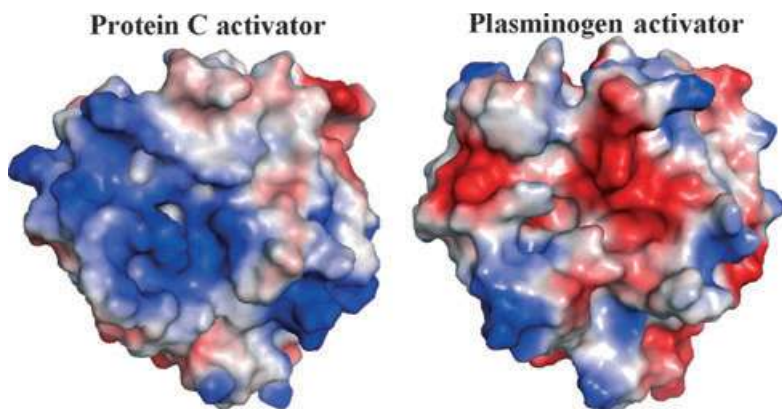
Fig. 10. Surface charge representations of the protein C activator and plasminogen activator in the regions of the active site gorges.

hole. Following the collapse of the tetrahedral intermediate and the expulsion of the leaving group, His57-H$^+$ plays the role of a general acid and the acyl–enzyme intermediate is formed. In the second step of the reaction, His57 deprotonates a water molecule which then interacts with the acyl–enzyme complex to yield a second tetrahedral intermediate, the collapse of which results in the liberation of the carboxylic acid product.

Zymogen activation

Activation of mammalian serine proteinases participating in digestion and the blood coagulation cascade, which are synthesized as inactive zymogens, requires the cleavage of the N-terminal peptide and additional cleavages in the regions 142–152, 184–193 and 216–223 [173]. This autocatalytic cleavage and subsequent removal of the N-terminal peptide results in the formation of a salt bridge between the new N-terminus and Asp194, and causes dramatic structural changes in both the S1 subsite and the oxyanion hole [177].

Since neither the activity of SVSP zymogens nor their structures have been determined, we can only infer the molecular mechanism involved in the maturation process. It is presumed that in the SVSPs, as in the case of trypsin, the S1 subsite and oxyanion hole are only formed upon cleavage and removal of this peptide since the N-terminal portion is conserved in snake and mammalian enzymes. Thus, as in the other serine proteinases, the loss of proteinase activity at high pH probably results from the deprotonation of the N-terminus and the disruption of the salt bridge, shifting the conformational equilibrium to resemble the inactive zymogen-like conformation [178].

Prothrombin activators

Serine proteinases which activate prothrombin are found exclusively in Australian snake venoms. The two groups differ in their co-factor requirements and structure: prothrombin activators consist of enzymes (e.g. trocarin D from *Tropidechis carinatus* venom) that require Ca^{2+}, FVa and negatively charged phospholipids for their optimal activities [179], whereas other enzymes (e.g. pseutarin C from *Pseudonaja textilis* venom) require Ca^{2+} and negatively charged phospholipids but not FVa for optimal activity [180]. Trocarin D is structurally and functionally similar to FXa; it has a light chain consisting of one Gla domain and two epidermal growth factor domains, linked by a single interchain disulfide bond to a heavy chain consisting of a serine proteinase domain [179]. In contrast, pseutarin C consists of two subunits, a catalytic subunit and a non-enzymatic subunit, which are structurally and functionally similar to FXa and FVa, respectively [181–183]. The catalytic subunit has similar light and heavy chains to trocarin D. The non-enzymatic subunit has a heavy chain (consisting of A1 and A2 domains) and a light chain (consisting of A3, C1 and C2 domains) that are held together by non-covalent interactions. Similar to FVa, the non-enzymatic subunit significantly increases the catalytic efficiency of the enzymatic subunit. Both these groups of prothrombin activators activate prothrombin by targeting the same cleavage sites as endogenous FXa and its complex with FVa. Thus these prothrombin activators are similar to blood coagulant factors and are probably evolved from blood coagulant factors by gene duplication [184–187].

Snake venom metalloproteinases (SVMPs)

It is estimated that SVMPs comprise at least 30% of the total protein of most viperid venoms [188]. SVMPs are primarily responsible for the hemorrhagic activity and the induction of local and systemic bleeding. SVMPs also possess diverse functions such as the dis-

ruption of hemostasis mediated by procoagulant or anticoagulant effects, platelet aggregation, and apoptotic or pro-inflammatory activities. Recent crystallographic studies of high-molecular-weight SVMPs and phylogenetically related ADAM (a disintegrin and metalloproteinase) and ADAMTS (ADAM with thrombospondin type-1 motif) family proteins have shed new light on the structure–function properties of this class of metalloproteinases.

Classification of SVMPs

SVMPs range in size from 20 to 100 kDa and are classified into three groups (P-I to P-III) according to their domain organization (Fig. 11A) [188,189]. P-I SVMPs are the simplest ones and they contain only a metalloproteinase (M) domain in their mature form. P-II SVMPs contain an M domain followed by a disintegrin (D) domain. In most cases, P-II SVMPs further
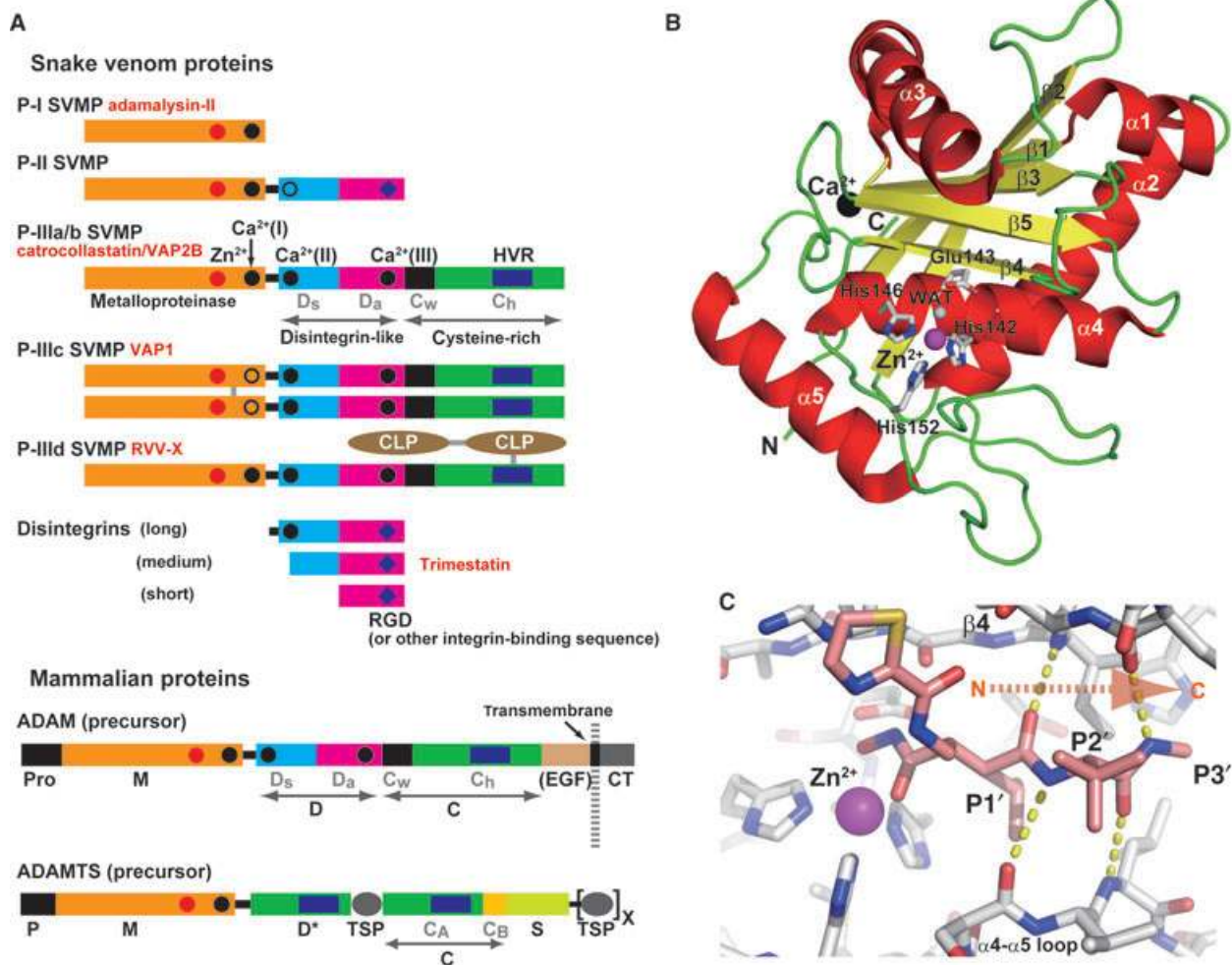
Fig. 11. The classification and structure of SVMPs. (A) Schematic representation of the domain structure of SVMPs, disintegrins and mammalian ADAM/ADAMTS family proteins. Each domain or subdomain is represented by a different color. CLP, C-type lectin-like domain; Pro, pro domain; CT, cytoplasmic domain; TSP, thrombospondin type-1 motif; EGF, epidermal growth factor like domain; S, spacer domain. The D domain of ADAMTSs does not possess a disintegrin-like structure but adopts an ADAMs' C_h-subdomain-like fold (see Fig. 13A) and thus is represented as D*. Calcium and zinc binding sites are schematically indicated. In VAP1, the ammonium group of Lys202 occupies the position of the calcium ion in the site I observed in other SVMPs. Some P-II SVMPs do not possess a calcium binding sequence at site II. ADAM10 and ADAM17 are atypical members of ADAMs as they lack calcium binding sites I and III and the EGF domain. (B) Ribbon structure of adamalysin II (PDB ID 1IAG), a structural prototype of P-I SVMPs. Zinc and calcium ions are represented as magenta and black spheres, respectively. (C) Close up view of the catalytic site of BaP-1 bound with the peptide mimetic inhibitor WR2 (PDB ID 2W12). The inhibitor (shown in light salmon) binds in an extended conformation closely mimicking the C-terminal part (P1′ to P3′ residues) of the enzyme-bound substrate. WR2 forms hydrogen bonds (represented by yellow dotted lines) with the adjacent β4 strand and the part of the loop connecting the α4 and α5 helices in BaP-1.

undergo proteolysis to produce non-enzymatic disintegrins that have strong platelet aggregation inhibitory activity. P-III SVMPs contain M, disintegrin-like (D) and cysteine-rich (C) domains. P-III SVMPs are further divided into subclasses based on their distinct post-translational modifications, such as dimerization (P-IIIc) or proteolytic processing (P-IIIb). The heterotrimeric subclass of SVMPs formerly called P-IV [189] is now included in the P-III group as a subclass (P-IIId), representing another post-translational modification of the canonical P-IIIa SVMPs [188]. All the classes have a signal (pre) and a pro domain sequence before the M domain in their gene structures, but none of the SVMPs with the pro domain has been isolated from the venom.

Related mammalian proteins

SVMPs are phylogenetically most closely related to ADAM family proteins and, together with ADAMs and ADAMTSs, constitute the adamalysin/reprolysin/ADAM family or M12B clan of zinc metalloproteinases (MEROPS classification, http://merops.sanger.ac.uk/).

ADAM family proteins are mammalian glycoproteins that have been implicated in cell–cell and cell–matrix association and signaling [190–193]. The best characterized *in vivo* activity of ADAMs is the ectodomain-shedding activity, which releases cell-surface-protein ectodomains including growth factors and cytokines, their receptors and cell adhesion molecules. ADAM17 was initially identified as the physiological convertase for tumor necrosis factor α [194,195]. In humans, 20 members of this family play key roles in development and homeostasis, as well as in pathological states including cancer, cardiovascular diseases, asthma and Alzheimer's disease [190–193]. Typical ADAMs are type-1 integral membrane proteins and have an epidermal-growth-factor-like domain, a transmembrane domain and a cytoplasmic domain, in addition to the metalloproteinase/disintegrin/cysteine-rich (MDC) domains (Fig. 11A).

The ADAMTS family proteinases have a modular structure similar to that of the ADAM family proteins, but they have a varying number of C-terminal thrombospondin type-1 repeats instead of a transmembrane/cytoplasmic segment, which identifies them as secreted proteinases (Fig. 11A). Nineteen members of this family have diverse functions including procollagen processing, aggrecan degradation, organogenesis and hemostasis in the human body [196,197]. Recent crystallographic studies have revealed that the D domains of ADAMTS proteins showed no structural homology to disintegrins but were very similar in

structure to part of the C domains of P-III SVMPs and ADAMs (see below) [198–201]. Thus, while the 'disintegrin-like' nomenclature has been used, ADAM-TSs actually have no disintegrin-like structures.

Crystal structures of SVMPs

Table S1 summarizes the structures of the adamalysin/reprolysin/ADAM family proteins determined by X-ray crystallography to date. The structure of adamalysin II, a non-hemorrhagic P-I SVMP isolated from *Crotalus adamantus*, is the first one to be resolved [202,203]. Crystal structures of nine P-I SVMPs are currently available in the Protein Data Bank (PDB). Vascular apoptosis-inducing protein-1 (VAP1) [204,205], a P-IIIc dimeric class SVMP isolated from *Crotalus atrox* venom, is the first P-III SVMP structure to be solved [206,207]. To date, structures of seven P-III SVMPs have been deposited in the PDB and they include almost all P-III subclass structures. P-II SVMP structures are currently unavailable, although an increasing number of crystal and solution structures of disintegrins are being added to the PDB.

Figure 11B depicts the crystal structure of adamalysin II, a structural prototype of the P-I class of SVMPs [202,203]. The M domain structures that are currently available for SVMPs (P-I and P-III classes), ADAMs and ADAMTSs can be superposed with each other with variability found only in the peripheral loop regions. The M domain has an oblate ellipsoidal shape with a notch in its flat side (Fig. 11B). The core of the M domain is formed by a five stranded β-sheet and five α-helices, and it contains the conserved Zn^{2+} binding <u>HEXXH</u>XXGXX<u>H</u>D sequence at the bottom of the catalytic gorge. The catalytic zinc ion is tetrahedrally coordinated by the three histidines and by a water molecule (Fig. 11B). The bound water molecule is polarized by the Glu residue and is involved in nucleophilic attack at the scissile peptide bond.

Crystal structures of SVMPs in complex with peptide-like inhibitors have shed light on the molecular mechanism of substrate recognition for catalysis (Fig. 11C) [208]. The inhibitor closely mimics the C-terminal part (P1′ to P3′) of an enzyme-bound substrate: the peptide-like inhibitor lies within the shallow catalytic gorge from left to right by forming hydrogen bonds with adjacent strands of the BaP-1 backbone in addition to a number of van der Waals contacts between the two molecules. The hydrogen bonding network between the enzyme and inhibitor resembles that of an antiparallel β-sheet, in essence extending the central β-sheet by two strands. Cleavage of basement membrane proteins with the consequent weakening of the

capillary structure is one of the mechanisms by which SVMPs induce hemorrhage [209]. Structural comparisons among SVMPs have revealed differences in the features of the substrate binding gorge in the M domain; however, no correlation between these structural differences and hemorrhagic activity has been found to date.

Figure 12A depicts the crystal structure of catrocollastatin/VAP2B from *C. atrox* venom, a structural prototype of the P-III class of SVMPs [210]. All the
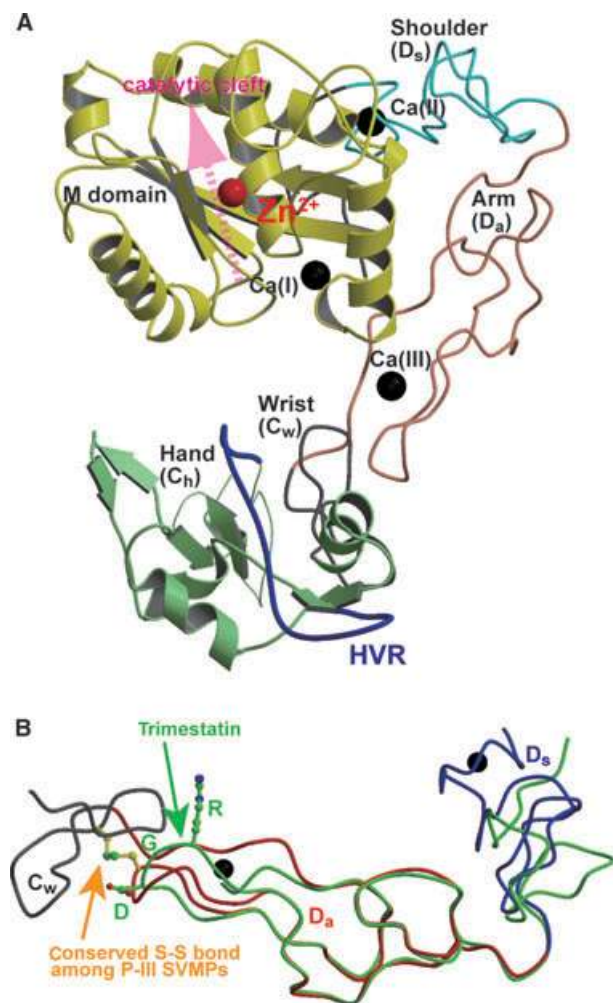
Fig. 12. The structure of a typical P-III SVMP. (A) Ribbon structure of catrocollastatin/VAP2B (A-chain of PDB ID 2DW0), a structural prototype of P-III SVMPs and ADAMs [210]. Zinc and calcium ions are represented as red and black spheres, respectively. Subdomains are shown in distinct colors A. (B) Superimposition of the D_a subdomain of catrocollastatin/VAP2B and RGD-containing disintegrin trimestatin (PDB ID 1J2L, shown in light green). The Arg-Gly-Asp side chains in trimestatin and the disulfide bond between the D_a and C_w subdomains in catrocollastatin/VAP2B, which is strictly conserved among the P-III SVMPs, are shown in ball-and-stick representation.

P-III SVMP structures revealed that the MDC domains fold into a C-shaped configuration in which the distal portion of the C domain comes close to the M domain catalytic site. Comparison of the available MDC structures revealed a substantial diversity in the relative orientation of the M and D domains, representing a dynamic property of the molecule that may be important for the function of this class of proteins [210,211]. Human ADAM22 also adopts essentially the same C-shaped configuration of the MDC domains as in the P-III SVMPs [212].

Within the C-shaped configuration of P-III SVMPs, the M domain is followed by the D domain, which protrudes from the M domain opposite to the catalytic site and close to the calcium binding site I (Fig. 12A).

Non-catalytic domains of P-III SVMPs

The D domain of P-III SVMPs is further divided into two structural subdomains named the 'shoulder' (D_s) and the 'arm' (D_a). These subdomains consist largely of a series of turns and constitute a continuous C-shaped arm structure together with the N-terminal portion of the C domain, which is designated the 'wrist' subdomain (C_w). The D_s and D_a subdomains contain structural calcium binding sites, sites II and III, respectively (Fig. 12A). There are three disulfide bonds in the D_s subdomain, three in D_a and one in C_w, and these subdomains are connected by a single disulfide bond. The residues coordinating the calcium ions and forming disulfide bonds are highly conserved among P-III SVMPs and ADAMs [206,207].

The structure of the D_a subdomain of the P-III SVMPs is quite similar to that of the RGD-containing disintegrin trimestatin [213] with the exception of the RGD-containing loop, designated 'disintegrin (D) loop', and the C-terminal region (Fig. 12B). These two regions are highly mobile, partly due to the absence of structural calcium ion in the core, and they are suggested candidate sites for integrin binding [214]. The D-loop in P-III SVMPs and ADAMs usually contains an XXCD sequence instead of the typical RGD motif. Using recombinant D domains or synthetic peptides, numerous P-III SVMPs and ADAMs have been shown to interact with particular integrins. However, crystal structures clearly indicate that the D-loop in P-III SVMPs and ADAMs is packed against the C_w subdomain, making the D-loop itself unavailable for protein–protein interactions due to steric hindrance. These findings highlight a discrepancy in the integrin binding hypothesis for P-III SVMPs and ADAMs. Therefore further studies are needed to elucidate whether and how the interactions with integrins observed in model

Fig. 13. Cysteine-rich (C) domain structures and potential protein–protein interaction sites. (A) Comparison of the C domain structures of SVMPs and mammalian counterparts. The C_h subdomains of VAP1 [206], RVV-X [211], human ADAM22 [212], bovine ADAM10 [215] and the D and C_A domains of human ADAMTS13 [200] are shown in ribbon representation. The conserved N-terminal α-helix, C-terminal β-strands and disulfide bonds are shown in red, yellow and orange, respectively. The V-loop and the HVR, which are suggested protein–protein interaction sites, are shown in gray and blue, respectively. Disordered regions within the crystals are shown as dotted lines. The N and C termini of the subdomains are indicated. The part of the light chain A in RVV-X is shown in light pink. The PDB accession code for each protein is indicated in parentheses. (B) Crystal structure of RVV-X in ribbon representation. Each domain or segment in the heavy chain is shown in the same color as in Fig. 11. The HVR of the RVV-X heavy chain is directly involved in the inter-subunit interaction. (C) Docking model. The molecular surfaces of RVV-X subdomains are colored as in (B). FXa is shown in ribbon representation. The side chain of the N-terminal Ile195 in the FXa heavy chain is shown in magenta. The concave gorge formed between the light chains may serve as the primary capture site for FX zymogen in the blood. The C_h/LA/LB portion may act as a scaffold to accommodate the elongated FX molecule, while separating the Gla domain and the scissile peptide bond. This relatively large separation between the catalytic site and the Gla-domain-binding exosite (~ 6.5 nm) may account for the high specificity of RVV-X for FX.

systems relate to the physiological functions of the P-III SVMPs.

The C-terminal region of the C domain of the P-III SVMPs, which is designated the 'hand' (C_h) subdomain, has a core made of a unique α⁄β-fold structure with no structural homology to currently known proteins other than the corresponding segments of ADAMs and ADAMTSs [198,201,206,212,215]. The whole C domain of the P-III SVMPs and ADAMs has

been deposited at the conserved domain database (CDD, http://www.ncbi.nlm.nih.gov/Structure/cdd/cdd.shtml) [216], as a member of the ADAM_CR Superfamily (cl02698). In addition to the D domain, the N-terminal portion of the C domain of ADAMTSs, designated the C_A subdomain, was recently found to adopt this ADAM_CR super-family fold [200]. Therefore, ADAMTSs have two ADAMs' C_h-subdomain-like folds separated by a thrombospondin type-1 motif within the molecule (Fig. 11A). Figure 13A represents a structural comparison of the C_h subdomains of SVMPs and ADAMs, and the corresponding portions of ADAMTSs. Despite low amino acid sequence identities (e.g. $\sim 15\%$ between VAP and ADAM10, $\sim 16\%$ between VAP1 and ADAMTS13 (D), and $\sim 17\%$ between the D and C_A domains of ADAM-TS13), they share a similar core structure and topology, including an N-terminal α-helix (shown in red), a C-terminal two-stranded β-sheet (shown in yellow), and four disulfide bonds (shown in orange). The peripheral loops, however, differ markedly in structure between these proteins.

The C_h subdomain's hyper-variable region (HVR, blue regions in Figs 12A and 13A) has been identified as the most variable in length and the area where the amino acid sequences are most divergent between SVMPs and ADAMs [206]. Different P-III SVMPs

have distinct HVR sequences, which result in distinct surface features. Therefore, they may function in specific protein–protein interactions, explaining the diversity of biological activities characteristic of this class of SVMPs. Because of its location within the molecule, opposite from the catalytic site (Fig. 12A), the HVR has been putatively assigned a protein binding and substrate recognition function [201,206].

Russell's viper venom FX activator (RVV-X)

RVV-X isolated from *Daboia russelli* venom is a member of the P-IIId SVMP family that consists of an MDC-containing heavy chain and two light chains of C-type lectin-like protein (Fig. 11A) [217–220]. RVV-X specifically activates FX by cleaving the same Arg194–Ile195 bond that is cleaved during physiological coagulation. FXa in turn converts prothrombin to thrombin, which ultimately leads to the formation of a hemostatic plug.

The crystal structure of RVV-X shows a hook–spanner–wrench-like architecture, in which the MD domains of the heavy chain constitute a hook, and the remainder of the molecule constitutes a handle [211] (Fig. 13B). The RVV-X heavy chain has a unique cysteine residue [Cys389 (H)] in the middle of the HVR. Cys389 forms a disulfide bond with the C-terminal cysteine residue of the light chain A [Cys133 (LA)] (Fig. 13A,B). In addition to this inter-chain disulfide bond, the HVR and surrounding residues form multiple hydrophobic interactions and hydrogen bonds, which further stabilize the continuous C_h/LA structure. The pseudo-symmetrical RVV-X light chain dimer is quite similar in structure to the FX binding protein (X-bp) from *Deinagkistrodon acutus* venom [221] that is solved in complex with the Gla domain of FX [222]. This structural similarity and previous biochemical observations suggest that the concave gorge formed by the light chains in RVV-X may function as an exosite for FX. A 6.5-nm separation between the catalytic site and the putative Gla-domain-binding exosite suggested a docking model for FXa [211,223] (Fig. 13C).

C-domain-mediated protein–protein interactions

The D/C domains may function to target P-III class SVMPs to their specific substrates, and they have therefore been suggested as the key structural determinants of potent hemorrhagic activity or diverse biological activities of this class of SVMPs. A substantial amount of isolated D/C-domain-containing fragments with specific toxicities has also been identified in the venoms that are probably the proteolytic products of

the processing of P-IIIb SVMPs. Jararhagin-C, catrocollastain-C and leberagin-C, which are D/C-domain-containing fragments isolated from *Bothrops jararaca*, *C. atrox* and *Macrovipera lebetina*, respectively, inhibit collagen-induced platelet aggregation [224–226]. Alternagin-C from *Bothrops alternatus* has been shown to modulate $\alpha_2\beta_1$ integrin-mediated cell adhesion, migration and proliferation [227]. The C domain of P-III SVMPS has not received the same level of attention as the D domain due to lack of structural information. The recombinant C domain of atrolysin A, another P-IIIa SVMP from *C. atrox* venom, specifically binds to collagen type I and von Willebrand factor (vWF), blocking collagen–vWF interactions [228,229] through the vWF A domain (vWA) [230]. This C domain also binds to vWA-like domain-containing extracellular matrix proteins, such as collagen XII, collagen XIV and matrilins 1, 3 and 4 [231]. However, the specific regions of the C domain involved in these interactions remain to be elucidated.

The resolution of the VAP1 and other structures has shed new light on the structure–function properties of P-III SVMPs and suggests a model in which the HVR constitutes an exosite that captures the target or associated proteins for processing by the catalytic site. The structure of RVV-X is consistent with this model and shows the first example of an HVR-mediated protein–protein interaction. In addition, this protease illustrates evolutionary gain of specificity in the P-III class SVMPs through the formation of an HVR-mediated exosite for the binding of specific substrates. Several reports suggest that the HVR directly contributes to the function of SVMPs. The peptide derived from the HVR of HF3, a hemorrhagic P-III SVMP from *B. jararaca*, promoted leukocyte rolling that was inhibited by anti-α_M/β_2 antibodies [232]. The peptides encompassing the HVR of jararhagin interfere with the interaction between platelets and collagen [233]. The peptide derived from the HVR of atragin inhibited cell migration [234]. Although these studies shed light on the functions of the HVR, short peptides do not always mimic their counterparts in the folded proteins. Additional structural and biochemical studies, including site-directed mutagenesis, will facilitate identification of the key substrates of individual SVMPs and enable a better understanding of the molecular mechanism of action of P-III SVMPs.

Functional role of the non-enzymatic proteins

In most cases, snake venom enzymes act as monomers and exhibit optimal pharmacological properties and

contribute to toxicity. At times, they form complexes with other non-enzymatic proteins to achieve higher efficiency through synergy. These non-enzymatic components play distinct functional roles in different complexes. In serine proteinase prothrombin activators (such as pseutarin C), a FVa-like non-enzymatic subunit enhances the V_{max} of the prothrombin activation reaction [181], whereas in procoagulant metalloproteinases (such as RVV-X and carinactivase), two light chains of C-type lectin-like protein contribute to specificity (FX and prothrombin, respectively) and Ca^{2+} dependence [235]. In ncHdPLA$_2$s, the basic components are toxic and induce a number of pharmacological effects, but the acidic subunits are neither toxic nor enzymatically active (or possess very low catalytic activity). These non-enzymatic subunits play distinct roles in different complexes. The crotoxin subunits dissociate when the complex interacts with synaptic membranes. The toxic PLA$_2$ binds to a specific membrane receptor while the non-toxic component remains in solution. The acidic subunit behaves as a 'chaperon' preventing a non-specific binding of the enzyme to other substrates and potentiates the toxicity [149]. The acidic component of viperotoxin F also potentiates the neurotoxicity of the basic subunit but reduces its enzymatic activity, while that of vipoxin plays a multifunctional role. It stabilizes the neurotoxic component of the complex preserving the toxicity for a long time, and decreases the neurotoxicity of the basic PLA$_2$ and its catalytic activity. In β-BTx, the covalently linked proteinase inhibitor-like subunit confers the target specificity by binding to voltage-dependent potassium channels [151]. Thus non-enzymatic components contribute significantly to the pharmacological efficiency of their respective enzymatic subunits. However, some questions are yet to be answered: why in some cases (crotoxin, viperotoxin F) does the acidic chain potentiate the toxicity but in others (vipoxin) reduce the pharmacological activity? How does the acidic subunit in vipoxin assist basic PLA$_2$ to switch the target from the presynaptic to postsynaptic side? Do they also affect other pharmacological effects of the toxic components?

Conclusions and future prospects

Venoms of snakes represent a veritable source of potent pharmacologically active molecules. The primary purpose of developing such a lethal concoction of toxins was probably for prey capture and defense, and venom proteins have certainly evolved to exhibit a plethora of novel pharmacological functions with impressive specificity and functions. Higher catalytic efficiency, heat stability and resistance to proteolysis as well as abundance of snake venom enzymes compared with non-venom homologs make them attractive models for biochemists, enzymologists and structural biologists. Despite sharing similar structural scaffolds, some of these enzyme toxins exhibit multiple pharmacological functions. Thus, structure–function relationships of such enzymes pose intriguing and exciting challenges to scientists. Structural studies of the enzymes have not only contributed to our understanding of the mechanism of catalysis but also to that of their inhibition. Using structural information, highly specific, nanomolar affinity inhibitory peptides have been designed successfully for PLA$_2$ enzymes. These encouraging initial successes will provide impetus. The inhibitors have significant importance in developing therapeutic prototypes and lead compounds for various human diseases and ailments (e.g. PLA$_2$ inhibitors as anti-inflammatory compounds, and metalloproteinase inhibitors as anti-metastatic compounds).

Acknowledgements

Author contributions

RKA and RMK coordinated and instituted the review by the multiple authors. TSK and RMK prepared the section on acetylcholinesterase, as well as doing the overall compilation and formatting of the manuscript. AV and ST prepared the sections on L-amino acid oxidase and snake venom metalloproteinase respectively. MTM and RKA prepared the section on snake venom serine proteinase. The section on phospholipase A$_2$, its inhibition by synthetic and natural inhibitors, and inhibitor design was prepared by SS, MS, SK, RPK, SD, PK, CB and TPS. CB, DG and NG prepared the section on heterodimeric PLA$_2$.

References

1 Menez A (1998) Functional architectures of animal toxins: a clue to drug design? *Toxicon* **36**, 1557–1572.

2 Kordis D & Gubensek F (2000) Adaptive evolution of animal toxin multigene families. *Gene* **261**, 43–52.

3 Frobert Y, Creminon C, Cousin X, Remy MH, Chatel JM, Bon S, Bon C & Grassi J (1997) Acetylcholinesterases from *Elapidae* snake venoms: biochemical, immunological and enzymatic characterization. *Biochim Biophys Acta* **1339**, 253–267.

4 Aldunate R, Casar JC, Brandan E & Inestrosa NC (2004) Structural and functional organization of synaptic acetylcholinesterase. *Brain Res Brain Res Rev* **47**, 96–104.

5 Bazelyansky M, Robey E & Kirsch JF (1986) Fractional diffusion-limited component of reactions catalyzed by acetylcholinesterase. *Biochemistry* **25**, 125–130.

6 Rothenberg MA & Nachmansohn D (1947) Studies on cholinesterase; purification of the enzyme from electric tissue by fractional ammonium sulfate precipitation. *J Biol Chem* **168**, 223–231.

7 Wilson IB & Harrison MA (1961) Turnover number of acetyl-cholinesterase. *J Biol Chem* **236**, 2292–2295.

8 Bon S, Vigny M & Massoulie J (1979) Asymmetric and globular forms of acetylcholinesterase in mammals and birds. *Proc Natl Acad Sci USA* **76**, 2546–2550.

9 Massoulie J, Pezzementi L, Bon S, Krejci E & Vallette FM (1993) Molecular and cellular biology of cholinesterases. *Prog Neurobiol* **41**, 31–91.

10 Massoulie J, Anselmet A, Bon S, Krejci E, Legay C, Morel N & Simon S (1998) Acetylcholinesterase: C-terminal domains, molecular forms and functional localization. *J Physiol Paris* **92**, 183–190.

11 Lyenger NK, Schra HB, Mukeiji B & Chopra RN (1938) Choline esterase in cobra venom. *Curr Sci India* **7**, 51–53.

12 Kumar V & Elliott WB (1973) The acetylcholinesterase of *Bungarus fasciatus* venom. *Eur J Biochem* **34**, 586–592.

13 Zeller EA (1948) Enzymes of snake venoms and their biological significance. *Adv Enzymol* **8**, 459–495.

14 Vigny M, Bon S, Massoulie J & Leterrier F (1978) Active-site catalytic efficiency of acetylcholinesterase molecular forms in *Electrophorus*, *Torpedo*, rat and chicken. *Eur J Biochem* **85**, 317–323.

15 Cousin X, Creminon C, Grassi J, Meflah K, Cornu G, Saliou B, Bon S, Massoulie J & Bon C (1996) Acetylcholinesterase from *Bungarus* venom: a monomeric species. *FEBS Lett* **387**, 196–200.

16 Cousin X, Bon S, Massoulie J & Bon C (1998) Identification of a novel type of alternatively spliced exon from the acetylcholinesterase gene of *Bungarus fasciatus*. Molecular forms of acetylcholinesterase in the snake liver and muscle. *J Biol Chem* **273**, 9812–9820.

17 Sussman JL, Harel M, Frolow F, Oefner C, Goldman A, Toker L & Silman I (1991) Atomic structure of acetylcholinesterase from *Torpedo californica*: a prototypic acetylcholine-binding protein. *Science* **253**, 872–879.

18 Taylor P & Radic Z (1994) The cholinesterases: from genes to proteins. *Annu Rev Pharmacol Toxicol* **34**, 281–320.

19 Barak D, Kronman C, Ordentlich A, Ariel N, Bromberg A, Marcus D, Lazar A, Velan B & Shafferman A (1994) Acetylcholinesterase peripheral anionic site degeneracy conferred by amino acid arrays sharing a common core. *J Biol Chem* **269**, 6296–6305.

20 Ordentlich A, Barak D, Kronman C, Ariel N, Segall Y, Velan B & Shafferman A (1995) Contribution of aromatic moieties of tyrosine 133 and of the anionic subsite tryptophan 86 to catalytic efficiency and allosteric modulation of acetylcholinesterase. *J Biol Chem* **270**, 2082–2091.

21 Eichler J, Anselment A, Sussman JL, Massoulie J & Silman I (1994) Differential effects of 'peripheral' site ligands on *Torpedo* and chicken acetylcholinesterase. *Mol Pharmacol* **45**, 335–340.

22 Ahmed M, Rocha JB, Morsch VM & Schetinger MR (2009) Snake venom acetylcholinesterase. In *Handbook of Venoms and Toxins of Reptiles* (Mackessy S ed), pp. 207–219. CRC Press, London.

23 Felder CE, Botti SA, Lifson S, Silman I & Sussman JL (1997) External and internal electrostatic potentials of cholinesterase models. *J Mol Graph Model* **15**, 318–327.

24 Johnson JL, Thomas JL, Emani S, Cusack B & Rosenberry TL (2005) Measuring carbamoylation and decarbamoylation rate constants by continuous assay of AChE. *Chem Biol Interact* **157–158**, 384–385.

25 Silman I & Sussman JL (2008) Acetylcholinesterase: how is structure related to function? *Chem Biol Interact* **175**, 3–10.

26 Radic Z, Pickering NA, Vellom DC, Camp S & Taylor P (1993) Three distinct domains in the cholinesterase molecule confer selectivity for acetyl- and butyrylcholinesterase inhibitors. *Biochemistry* **32**, 12074–12084.

27 Bourne Y, Taylor P & Marchot P (1995) Acetylcholinesterase inhibition by fasciculin: crystal structure of the complex. *Cell* **83**, 503–512.

28 Rodrigues RS, da Silva JF, Boldrini Franca J, Fonseca FP, Otaviano AR, Henrique Silva F, Hamaguchi A, Magro AJ, Braz AS, dos Santos JI *et al.* (2009) Structural and functional properties of Bp-LAAO, a new L-amino acid oxidase isolated from *Bothrops pauloensis* snake venom. *Biochimie* **91**, 490–501.

29 Zhong SR, Jin Y, Wu JB, Jia YH, Xu GL, Wang GC, Xiong YL & Lu QM (2009) Purification and character-

ization of a new L-amino acid oxidase from *Daboia russellii siamensis* venom. *Toxicon* **54**, 763–771.

30 Braga MD, Martins AM, Amora DN, de Menezes DB, Toyama MH, Toyama DO, Marangoni S, Alves CD, Barbosa PS, de Sousa Alves R *et al.* (2008) Purification and biological effects of L-amino acid oxidase isolated from *Bothrops insularis* venom. *Toxicon* **51**, 199–207.

31 Jin Y, Lee WH, Zeng L & Zhang Y (2007) Molecular characterization of L-amino acid oxidase from king cobra venom. *Toxicon* **50**, 479–489.

32 Ponnudurai G, Chung MCM & Tan N-H (1994) Purification and properties of the L-amino acid oxidase from Malayan pit viper (*Calloselasma rhodostoma*) venom. *Arch Biochem Biophy* **313**, 373–378.

33 Tong H, Chen W, Shi W, Qi F & Dong X (2008) SO-LAAO, a novel L-amino acid oxidase that enables *Streptococcus oligofermentans* to outcompete *Streptococcus mutans* by generating H_2O_2 from peptone. *J Bacteriol* **190**, 4716–4721.

34 Arima J, Sasaki C, Sakaguchi C, Mizuno H, Tamura T, Kashima A, Kusakabe H, Sugio S & Inagaki K (2009) Structural characterization of L-glutamate oxidase from *Streptomyces* sp. X-119-6. *FEBS Journal* **276**, 3894–3903.

35 Braun M, Kim JM & Schmid RD (1992) Purification and some properties of an extracellular L-amino acid oxidase from *Cellulomonas cellulans* AM8 isolated from soil. *Appl Microbiol Biotechnol* **37**, 594–598.

36 Brearley GM, Price CP, Atkinson T & Hammond PM (1994) Purification and partial characterization of a broad-range L-amino acid oxidase from *Bacillus carotarum* 2Pfa isolated from soil. *Appl Microbiol Biotechnol* **41**, 670–676.

37 Kusakabe H, Kodama K, Kuninaka A, Yoshino H, Misono H & Soda K (1980) A new antitumor enzyme, L-lysine alpha-oxidase from *Trichoderma viride*. Purification and enzymological properties. *J Biol Chem* **255**, 976–981.

38 Le KH & Villanueva VR (1978) Purification and characterization of epsilon-*N*-trimethyllysine L-amino oxidase from *Neurospora crassa*. *Biochim Biophys Acta* **524**, 288–296.

39 Piedras P, Pineda M, Munoz J & Cardenas J (1992) Purification and characterizatino of an L-amino acid oxidase from *Chlamydomonas reinhardtii*. *Planta* **188**, 13–18.

40 de Kok A & Rawitch AB (1969) Studies on L-amino acid oxidase. II. Dissociation and characterization of its subunits. *Biochemistry* **8**, 1405–1411.

41 de Kok A & Veeger C (1968) Studies on L-amino acid oxidase. I. Effects of pH and competitive inhibitors. *Biochim Biophys Acta* **167**, 35–47.

42 Massey V & Curti B (1967) On the reaction mechanism of *Crotalus adamanteus* L-amino acid oxidase. *J Biol Chem* **242**, 1259–1264.

43 Wellner D (1966) Evidence for conformational changes in L-amino acid oxidase associated with reversible inactivation. *Biochemistry* **5**, 1585–1591.

43a Kearney EB & Singer TP (1951a) The L-amino acid oxidases of snake venom. III. Reversible inactivation of L-amino acid oxidases. *Arch Biochem* **33**, 377–396.

43b Kearney EB & Singer TP (1951b) The L-amino acid oxidases of snake venom. IV. The effect of anions on the reversible inactivation. *Arch Biochem* **33**, 397–343.

43c Kearney EB & Singer TP (1951c) The L-amino acid oxidases of snake venom. V. Mechanism of the reversible inactivation. *Arch Biochem* **33**, 414–426.

44 Curti B, Massey V & Zmudka M (1968) Inactivation of snake venom L-amino acid oxidase by freezing. *J Biol Chem* **243**, 2306–2314.

45 Pawelek P, Cheah J, Coulombe R, Macheroux P, Ghisla S & Vrielink A (2000) The structure of L-amino acid oxidase reveals the substrate trajectory into an enantiomerically conserved active site. *EMBO J* **19**, 4204–4215.

46 Eventoff W & Rossmann MG (1975) The evolution of dehydrogenases and kinases. *CRC Crit Rev Biochem* **3**, 111–140.

47 Ohlsson I, Nordstrom B & Branden CI (1974) Structural and functional similarities within the coenzyme binding domains of dehydrogenases. *J Mol Biol* **89**, 339–354.

48 Hol WG, van Duijnen PT & Berendsen HJ (1978) The alpha-helix dipole and the properties of proteins. *Nature* **273**, 443–446.

49 Moustafa IM, Foster S, Lyubimov AY & Vrielink A (2006) Crystal structure of LAAO from *Calloselasma rhodostoma* with an L-phenylalanine substrate: insights into structure and mechanism. *J Mol Biol* **364**, 991–1002.

50 Umhau S, Diederichs K, Welte W, Ghisla S, Pollegioni L, Molla G, Porrini D & Pilone MS (1999) Very high resoution crystal structure of D-amino acid oxidase. Insights into the reaction mechanisms and mode of ligand binding. In *Flavins and Flavoproteins* (Ghisla S, Kroneck P, Macheroux P & Sund H eds), pp. 567–570. Ruldolf Weber, Berlin.

51 Zhang H, Teng M, Niu L, Wang Y, Liu Q, Huang Q, Hao Q, Dong Y & Liu P (2004) Purification, partial characterization, crystallization and structural determination of AHP-LAAO, a novel L-amino-acid oxidase with cell apoptosis-inducing activity from *Agkistrodon halys pallas* venom. *Acta Crystallogr D Biol Crystallogr* **60**, 974–977.

52 Faust A, Niefind K, Hummel W & Schomburg D (2007) The structure of a bacterial L-amino acid oxidase from *Rhodococcus opacus* gives new evidence fot the hydride mechanism for dehydrogenation. *J Mol Biol* **367**, 234–248.

53 Ida K, Kurabayashi M, Suguro M, Hiruma Y, Hikima T, Yamomoto M & Suzuki H (2008) Structural basis

of proteolytic activation of L-phenylalanine oxidase from *Pseudomonas* sp. P-501. *J Biol Chem* **283**, 16584–16590.

54 Nathan I, Dvilansky A, Yirmiyahu T, Aharon M & Livne A (1982) Impairment of platelet aggregation by *Echis colorata* venom mediated by L-amino acid oxidase or H_2O_2. *Thromb Haemost* **48**, 277–282.

55 Sakurai Y, Takatsuka H, Yoshioka A, Matsui T, Suzuki M, Titani K & Fujimura Y (2001) Inhibition of human platelet aggregation by L-amino acid oxidase purified from *Naja naja kaouthia* venom. *Toxicon* **39**, 1827–1833.

56 Takatsuka H, Sakurai Y, Yoshioka A, Kokubo T, Usami Y, Suzuki M, Matsui T, Titani K, Yagi H, Matsumoto M *et al.* (2001) Molecular characterization of L-amino acid oxidase from *Agkistrodon halys blomhoffii* with special reference to platelet aggregation. *Biochim Biophys Acta* **1544**, 267–277.

57 Li ZY, Yu TF & Lian EC (1994) Purification and characterization of L-amino acid oxidase from king cobra (*Ophiophagus hannah*) venom and its effects on human platelet aggregation. *Toxicon* **32**, 1349–1358.

58 Lu QM, Wei Q, Jin Y, Wei JF, Wang WY & Xiong YL (2002) L-Amino acid oxidase from *Trimeresurus jerdonii* snake venom: purification, characterization, platelet aggregation-inducing and antibacterial effects. *J Nat Toxins* **11**, 345–352.

59 Stabeli RG, Marcussi S, Carlos GB, Pietro RC, Selistre-de-Araujo HS, Giglio JR, Oliveira EB & Soares AM (2004) Platelet aggregation and antibacterial effects of an L-amino acid oxidase purified from *Bothrops alternatus* snake venom. *Bioorg Med Chem* **12**, 2881–2886.

60 Araki S, Ishida T, Yamamoto T, Kaji K & Hayashi H (1993) Induction of apoptosis by hemorrhagic snake venom in vascular endothelial cells. *Biochem Biophys Res Commun* **190**, 148–153.

61 Suhr SM & Kim DS (1996) Identification of the snake venom substance that induces apoptosis. *Biochem Biophys Res Commun* **224**, 134–139.

62 Torii S, Naito M & Tsuruo T (1997) Apoxin I, a novel apoptosis-inducing factor with L-amino acid oxidase activity purified from Western diamondback rattlesnake venom. *J Biol Chem* **272**, 9539–9542.

63 Ande SR, Kommoju PR, Draxl S, Murkovic M, Macheroux P, Ghisla S & Ferrando-May E (2006) Mechanisms of cell death induction by L-amino acid oxidase, a major component of ophidian venom. *Apoptosis* **11**, 1439–1451.

64 Suhr SM & Kim DS (1999) Comparison of the apoptotic pathways induced by L-amino acid oxidase and hydrogen peroxide. *J Biochem* **125**, 305–309.

65 Du XY & Clemetson KJ (2002) Snake venom L-amino acid oxidases. *Toxicon* **40**, 659–665.

66 Geyer A, Fitzpatrick TB, Pawelek PD, Kitzing K, Vrielink A, Ghisla S & Macheroux P (2001) Structure and characterization of the glycan moiety of L-amino-acid oxidase from the Malayan pit viper *Calloselasma rhodostoma*. *Eur J Biochem* **268**, 4044–4053.

67 Burke JE & Dennis EA (2009) Phospholipase A_2 biochemistry. *Cardiovasc Drugs Ther* **23**, 49–59.

68 Kudo I & Murakami M (2002) Phospholipase A_2 enzymes. *Prostaglandins Other Lipid Mediat* **68–69**, 3–58.

69 Smith GM, Ward RL, McGuigan L, Rajkovic IA & Scott KF (1992) Measurement of human phospholipase A_2 in arthritis plasma using a newly developed sandwich ELISA. *Br J Rheumatol* **31**, 175–178.

70 Waite M (1987) *Handbook of Lipid Research*. Plenum Press, New York.

71 Burke JE & Dennis EA (2009) Phospholipase A_2 structure/function, mechanism, and signaling. *J Lipid Res* **50**(Suppl), S237–242.

72 Schaloske RH & Dennis EA (2006) The phospholipase A_2 superfamily and its group numbering system. *Biochim Biophys Acta* **1761**, 1246–1259.

73 Heinrikson RL, Krueger ET & Keim PS (1977) Amino acid sequence of phospholipase A_2-alpha from the venom of *Crotalus adamanteus*. A new classification of phospholipases A2 based upon structural determinants. *J Biol Chem* **252**, 4913–4921.

74 Kini RM (1997) Phospholipase A_2 – a complex multifunctional protein puzzle. In *Venom Phospholipase A2 Enzymes: Structure, Function and Mechanism* (Kini RM ed), pp. 1–28. Wiley, Chichester.

75 Kini RM (2006) Anticoagulant proteins from snake venoms: structure, function and mechanism. *Biochem J* **397**, 377–387.

76 Santos-Filho NA, Silveira LB, Oliveira CZ, Bernardes CP, Menaldo DL, Fuly AL, Arantes EC, Sampaio SV, Mamede CC, Beletti ME *et al.* (2008) A new acidic myotoxic, anti-platelet and prostaglandin I_2 inductor phospholipase A_2 isolated from *Bothrops moojeni* snake venom. *Toxicon* **52**, 908–917.

77 Shipolini RA, Callewaert GL, Cottrell RC & Vernon CA (1974) The amino-acid sequence and carbohydrate content of phospholipase A_2 from bee venom. *Eur J Biochem* **48**, 465–476.

78 Valdez-Cruz NA, Batista CV & Possani LD (2004) Phaiodactylipin, a glycosylated heterodimeric phospholipase A from the venom of the scorpion *Anuroctonus phaiodactylus*. *Eur J Biochem* **271**, 1453–1464.

79 Welches W, Felsher D, Landshulz W & Maraganore JM (1985) A rapid method for the purification of monomeric and/or dimeric phospholipases A_2 in crotalid snake venoms. *Toxicon* **23**, 747–754.

80 Seilhamer JJ, Randall TL, Yamanaka M & Johnson LK (1986) Pancreatic phospholipase A_2: isolation of the human gene and cDNAs from porcine pancreas and human lung. *DNA* **5**, 519–527.

81 Six DA & Dennis EA (2000) The expanding superfamily of phospholipase A(2) enzymes: classification and characterization. *Biochim Biophys Acta* **1488**, 1–19.

82 Kramer RM & Pepinsky RB (1991) Assay and purification of phospholipase A_2 from human synovial fluid in rheumatoid arthritis. *Methods Enzymol* **197**, 373–381.

83 Seilhamer JJ, Plant S, Pruzanski W, Schilling J, Stefanski E, Vadas P & Johnson LK (1989) Multiple forms of phospholipase A_2 in arthritic synovial fluid. *J Biochem* **106**, 38–42.

84 Berg OG, Gelb MH, Tsai MD & Jain MK (2001) Interfacial enzymology: the secreted phospholipase A(2)-paradigm. *Chem Rev* **101**, 2613–2654.

85 Ray S, Scott JL & Tatulian SA (2007) Effects of lipid phase transition and membrane surface charge on the interfacial activation of phospholipase A_2. *Biochemistry* **46**, 13089–13100.

86 Carman GM, Deems RA & Dennis EA (1995) Lipid signaling enzymes and surface dilution kinetics. *J Biol Chem* **270**, 18711–18714.

87 Gelb MH, Jain MK, Hanel AM & Berg OG (1995) Interfacial enzymology of glycerolipid hydrolases: lessons from secreted phospholipases A_2. *Annu Rev Biochem* **64**, 653–688.

88 Balasubramanya R, Chandra V, Kaur P & Singh TP (2005) Crystal structure of the complex of the secretory phospholipase A_2 from *Daboia russelli pulchella* with an endogenic indole derivative, 2-carbamoylmethyl-5-propyl-octahydro-indol-7-yl-acetic acid at 1.8 Å resolution. *Biochim Biophys Acta* **1752**, 177–185.

89 Chandra V, Jasti J, Kaur P, Betzel C, Srinivasan A & Singh TP (2002) First structural evidence of a specific inhibition of phospholipase A_2 by alpha-tocopherol (vitamin E) and its implications in inflammation: crystal structure of the complex formed between phospholipase A_2 and alpha-tocopherol at 1.8 Å resolution. *J Mol Biol* **320**, 215–222.

90 Chandra V, Jasti J, Kaur P, Dey S, Perbandt M, Srinivasan A, Betzel C & Singh TP (2002) Crystal structure of a complex formed between a snake venom phospholipase A(2) and a potent peptide inhibitor Phe-Leu-Ser-Tyr-Lys at 1.8 Å resolution. *J Biol Chem* **277**, 41079–41085.

91 Chandra V, Jasti J, Kaur P, Srinivasan A, Betzel C & Singh TP (2002) Structural basis of phospholipase A_2 inhibition for the synthesis of prostaglandins by the plant alkaloid aristolochic acid from a 1.7 Å crystal structure. *Biochemistry* **41**, 10914–10919.

92 Chandra V, Kaur P, Jasti J, Betzel C & Singh TP (2001) Regulation of catalytic function by molecular

association: structure of phospholipase A_2 from *Daboia russelli pulchella* (DPLA2) at 1.9 Å resolution. *Acta Crystallogr D Biol Crystallogr* **57**, 1793–1798.

93 Chandra V, Kaur P, Srinivasan A & Singh TP (2000) Three-dimensional structure of a presynaptic neurotoxic phospholipase A_2 from *Daboia russelli pulchella* at 2.4 Å resolution. *J Mol Biol* **296**, 1117–1126.

94 Fremont DH, Anderson DH, Wilson IA, Dennis EA & Xuong NH (1993) Crystal structure of phospholipase A_2 from Indian cobra reveals a trimeric association. *Proc Natl Acad Sci USA* **90**, 342–346.

95 Gu L, Zhang H, Song S, Zhou Y & Lin Z (2002) Structure of an acidic phospholipase A_2 from the venom of *Deinagkistrodon acutus*. *Acta Crystallogr D Biol Crystallogr* **58**, 104–110.

96 Jabeen T, Singh N, Singh RK, Ethayathulla AS, Sharma S, Srinivasan A & Singh TP (2005) Crystal structure of a novel phospholipase A_2 from *Naja naja sagittifera* with a strong anticoagulant activity. *Toxicon* **46**, 865–875.

97 Jasti J, Paramasivam M, Srinivasan A & Singh TP (2004) Structure of an acidic phospholipase A_2 from Indian saw-scaled viper (*Echis carinatus*) at 2.6 Å resolution reveals a novel intermolecular interaction. *Acta Crystallogr D Biol Crystallogr* **60**, 66–72.

98 Lok SM, Gao R, Rouault M, Lambeau G, Gopalakrishnakone P & Swaminathan K (2005) Structure and function comparison of *Micropechis ikaheka* snake venom phospholipase A_2 isoenzymes. *FEBS J* **272**, 1211–1220.

99 Perbandt M, Wilson JC, Eschenburg S, Mancheva I, Aleksiev B, Genov N, Willingmann P, Weber W, Singh TP & Betzel C (1997) Crystal structure of vipoxin at 2.0 Å: an example of regulation of a toxic function generated by molecular evolution. *FEBS Lett* **412**, 573–577.

100 Singh G, Gourinath S, Sharma S, Paramasivam M, Srinivasan A & Singh TP (2001) Sequence and crystal structure determination of a basic phospholipase A_2 from common krait (*Bungarus caeruleus*) at 2.4 Å resolution: identification and characterization of its pharmacological sites. *J Mol Biol* **307**, 1049–1059.

101 Singh G, Jasti J, Saravanan K, Sharma S, Kaur P, Srinivasan A & Singh TP (2005) Crystal structure of the complex formed between a group I phospholipase A_2 and a naturally occurring fatty acid at 2.7 Å resolution. *Protein Sci* **14**, 395–400.

102 Tang L, Zhou YC & Lin ZJ (1998) Crystal structure of agkistrodotoxin, a phospholipase A_2-type presynaptic neurotoxin from *Agkistrodon halys pallas*. *J Mol Biol* **282**, 1–11.

103 Xu S, Gu L, Jiang T, Zhou Y & Lin Z (2003) Structures of cadmium-binding acidic phospholipase A_2 from the venom of *Agkistrodon halys pallas* at 1.9 Å

resolution. *Biochem Biophys Res Commun* **300**, 271–277.

104 Xu S, Gu L, Wang Q, Shu Y, Song S & Lin Z (2003) Structure of a king cobra phospholipase A₂ determined from a hemihedrally twinned crystal. *Acta Crystallogr D Biol Crystallogr* **59**, 1574–1581.

105 Jabeen T, Singh N, Singh RK, Jasti J, Sharma S, Kaur P, Srinivasan A & Singh TP (2006) Crystal structure of a heterodimer of phospholipase A₂ from *Naja naja sagittifera* at 2.3 Å resolution reveals the presence of a new PLA2-like protein with a novel cys 32-Cys 49 disulphide bridge with a bound sugar at the substrate-binding site. *Proteins* **62**, 329–337.

106 Kugiyama K, Ota Y, Takazoe K, Moriyama Y, Kawano H, Miyao Y, Sakamoto T, Soejima H, Ogawa H, Doi H *et al.* (1999) Circulating levels of secretory type II phospholipase A(2) predict coronary events in patients with coronary artery disease. *Circulation* **100**, 1280–1284.

107 Webb NR, Bostrom MA, Szilvassy SJ, van der Westhuyzen DR, Daugherty A & de Beer FC (2003) Macrophage-expressed group IIA secretory phospholipase A₂ increases atherosclerotic lesion formation in LDL receptor-deficient mice. *Arterioscler Thromb Vasc Biol* **23**, 263–268.

108 Banumathi S, Rajashankar KR, Notzel C, Aleksiev B, Singh TP, Genov N & Betzel C (2001) Structure of the neurotoxic complex vipoxin at 1.4 Å resolution. *Acta Crystallogr D Biol Crystallogr* **57**, 1552–1559.

109 Wery JP, Schevitz RW, Clawson DK, Bobbitt JL, Dow ER, Gamboa G, Goodson T Jr, Hermann RB, Kramer RM, McClure DB *et al.* (1991) Structure of recombinant human rheumatoid arthritic synovial fluid phospholipase A₂ at 2.2 Å resolution. *Nature* **352**, 79–82.

110 Cha SS, Lee D, Adams J, Kurdyla JT, Jones CS, Marshall LA, Bolognese B, Abdel-Meguid SS & Oh BH (1996) High-resolution X-ray crystallography reveals precise binding interactions between human nonpancreatic secreted phospholipase A₂ and a highly potent inhibitor (FPL67047XX). *J Med Chem* **39**, 3878–3881.

111 Chandra V, Jasti J, Kaur P, Dey S, Srinivasan A, Betzel C & Singh TP (2002) Design of specific peptide inhibitors of phospholipase A₂: structure of a complex formed between Russell's viper phospholipase A₂ and a designed peptide Leu-Ala-Ile-Tyr-Ser (LAIYS). *Acta Crystallogr D Biol Crystallogr* **58**, 1813–1819.

112 Hansford KA, Reid RC, Clark CI, Tyndall JD, Whitehouse MW, Guthrie T, McGeary RP, Schafer K, Martin JL & Fairlie DP (2003) D-Tyrosine as a chiral precursor to potent inhibitors of human nonpancreatic secretory phospholipase A₂ (IIa) with antiinflammatory activity. *Chembiochem* **4**, 181–185.

113 Kitadokoro K, Hagishita S, Sato T, Ohtani M & Miki K (1998) Crystal structure of human secretory phospholipase A₂-IIA complex with the potent indolizine inhibitor 120-1032. *J Biochem* **123**, 619–623.

114 Schevitz RW, Bach NJ, Carlson DG, Chirgadze NY, Clawson DK, Dillard RD, Draheim SE, Hartley LW, Jones ND, Mihelich ED *et al.* (1995) Structure-based design of the first potent and selective inhibitor of human non-pancreatic secretory phospholipase A₂. *Nat Struct Biol* **2**, 458–465.

115 Scott DL, White SP, Browning JL, Rosa JJ, Gelb MH & Sigler PB (1991) Structures of free and inhibited human secretory phospholipase A₂ from inflammatory exudate. *Science* **254**, 1007–1010.

116 Singh N, Jabeen T, Pal A, Sharma S, Perbandt M, Betzel C & Singh TP (2006) Crystal structures of the complexes of a group IIA phospholipase A₂ with two natural anti-inflammatory agents, anisic acid, and atropine reveal a similar mode of binding. *Proteins* **64**, 89–100.

117 Singh N, Jabeen T, Sharma S, Somvanshi RK, Dey S, Srinivasan A & Singh TP (2006) Specific binding of non-steroidal anti-inflammatory drugs (NSAIDs) to phospholipase A₂: structure of the complex formed between phospholipase A2 and diclofenac at 2.7 Å resolution. *Acta Crystallogr D Biol Crystallogr* **62**, 410–416.

118 Singh N, Kumar RP, Kumar S, Sharma S, Mir R, Kaur P, Srinivasan A & Singh TP (2009) Simultaneous inhibition of anti-coagulation and inflammation: crystal structure of phospholipase A₂ complexed with indomethacin at 1.4 Å resolution reveals the presence of the new common ligand-binding site. *J Mol Recognit* **22**, 437–445.

119 Blow D (1990) Enzymology. More of the catalytic triad. *Nature* **343**, 694–695.

120 Dessen A, Tang J, Schmidt H, Stahl M, Clark JD, Seehra J & Somers WS (1999) Crystal structure of human cytosolic phospholipase A₂ reveals a novel topology and catalytic mechanism. *Cell* **97**, 349–360.

121 Bernard P, Pintore M, Berthon JY & Chretien JR (2001) A molecular modeling and 3D QSAR study of a large series of indole inhibitors of human non-pancreatic secretory phospholipase A₂. *Eur J Med Chem* **36**, 1–19.

122 Scott DL, White SP, Otwinowski Z, Yuan W, Gelb MH & Sigler PB (1990) Interfacial catalysis: the mechanism of phospholipase A₂. *Science* **250**, 1541–1546.

123 Singh N, Jabeen T, Somvanshi RK, Sharma S, Dey S & Singh TP (2004) Phospholipase A₂ as a target protein for nonsteroidal anti-inflammatory drugs (NSAIDS): crystal structure of the complex formed between phospholipase A₂ and oxyphenbutazone at 1.6 Å resolution. *Biochemistry* **43**, 14577–14583.

124 Castoe TA & Parkinson CL (2006) Bayesian mixed models and the phylogeny of pitvipers (Viperidae: Serpentes). *Mol Phylogenet Evol* **39**, 91–110.

125 Aird SD, Kaiser II, Lewis RV & Kruggel WG (1985) Rattlesnake presynaptic neurotoxins: primary structure and evolutionary origin of the acidic subunit. *Biochemistry* **24**, 7054–7058.

126 Bouchier C, Boulain JC, Bon C & Menez A (1991) Analysis of cDNAs encoding the two subunits of crotoxin, a phospholipase A_2 neurotoxin from rattlesnake venom: the acidic non enzymatic subunit derives from a phospholipase A_2-like precursor. *Biochim Biophys Acta* **1088**, 401–408.

127 Bon C & Jeng TW (1979) Crotoxin: a possible mechanism of action. *Adv Cytopharmacol* **3**, 231–235.

128 Choumet V, Saliou B, Fideler L, Chen YC, Gubensek F, Bon C & Delot E (1993) Snake-venom phospholipase A_2 neurotoxins. Potentiation of a single-chain neurotoxin by the chaperon subunit of a two-component neurotoxin. *Eur J Biochem* **211**, 57–62.

129 Aleksiev B & Tchorbanov B (1976) Action on phosphatidylcholine of the toxic phospholipase A_2 from the venom of bulgarian viper (*Vipera ammodytes ammodytes*). *Toxicon* **14**, 477–485.

130 Bon C (1997) Multicomponent neurotoxic phospholipase A_2. In *Venom Phospholipase A2: Structure, Function and Mechanism* (Kini RM ed), pp. 269–286. Wiley, Chichester.

131 Santos KF, Murakami MT, Cintra AC, Toyama MH, Marangoni S, Forrer VP, Brandao Neto JR, Polikarpov I & Arni RK (2007) Crystallization and preliminary X-ray crystallographic analysis of the heterodimeric crotoxin complex and the isolated subunits crotapotin and phospholipase A_2. *Acta Crystallogr Sect F Struct Biol Cryst Commun* **63**, 287–290.

132 Abrego JR, Craievich AF, Mascarenhas YP & Laure CJ (1993) SAXS study of crotapotin at low pH. *Biophys J* **64**, 560–564.

133 Marchi-Salvador DP, Correa LC, Magro AJ, Oliveira CZ, Soares AM & Fontes MR (2008) Insights into the role of oligomeric state on the biological activities of crotoxin: crystal structure of a tetrameric phospholipase A_2 formed by two isoforms of crotoxin B from *Crotalus durissus terrificus* venom. *Proteins* **72**, 883–891.

134 Chen YH, Wang YM, Hseu MJ & Tsai IH (2004) Molecular evolution and structure-function relationships of crotoxin-like and asparagine-6-containing phospholipases A_2 in pit viper venoms. *Biochem J* **381**, 25–34.

135 Gopalakrishnakone P, Hawgood BJ, Holbrooke SE, Marsh NA, Santana De Sa S & Tu AT (1980) Sites of action of Mojave toxin isolated from the venom of the Mojave rattlesnake. *Br J Pharmacol* **69**, 421–431.

136 Mallow D, Ludwig D & Nilson G (2003) *True Vipers: Natural History and Toxinology of Old World Vipers*. Krieger Publishing, Malabar, FL.

137 Aleksiev B & Shipolini R (1971) [Further studies on the fractionation and purification of the toxic components from the venom of the Bulgarian viper (*Vipera ammodytes ammodytes*)]. *Hoppe Seylers Z Physiol Chem* **352**, 1183–1188.

138 Tchorbanov B, Grishin E, Aleksiev B & Ovchinnikov Y (1978) A neurotoxic complex from the venom of the Bulgarian viper (*Vipera ammodytes ammodytes*) and partial amino acid sequence of the toxic phospholipase A_2. *Toxicon* **16**, 37–44.

139 Mancheva I, Kleinschmidt T, Aleksiev B & Braunitzer G (1987) Sequence homology between phospholipase and its inhibitor in snake venom. The primary structure of phospholipase A2 of vipoxin from the venom of the Bulgarian viper (Vipera ammodytes ammodytes, Serpentes). *Biol Chem Hoppe Seyler* **368**, 343–352.

140 Betzel C, Genov N, Rajashankar KR & Singh TP (1999) Modulation of phospholipase A_2 activity generated by molecular evolution. *Cell Mol Life Sci* **56**, 384–397.

141 Renetseder R, Dijkstra BW, Huizinga K, Kalk KH & Drenth J (1988) Crystal structure of bovine pancreatic phospholipase A_2 covalently inhibited by *p*-bromophenacyl-bromide. *J Mol Biol* **200**, 181–188.

142 Georgieva DN, Genov N, Hristov K, Dierks K & Betzel C (2004) Interactions of the neurotoxin vipoxin in solution studied by dynamic light scattering. *Biophys J* **86**, 461–466.

143 Georgieva DN, Rypniewski W, Gabdoulkhakov A, Genov N & Betzel C (2004) Asp49 phospholipase A(2)-elaidoylamide complex: a new mode of inhibition. *Biochem Biophys Res Commun* **319**, 1314–1321.

144 Georgieva DN, Perbandt M, Rypniewski W, Hristov K, Genov N & Betzel C (2004) The X-ray structure of a snake venom Gln48 phospholipase A_2 at 1.9 Å resolution reveals anion-binding sites. *Biochem Biophys Res Commun* **316**, 33–38.

145 Wang YM, Lu PJ, Ho CL & Tsai IH (1992) Characterization and molecular cloning of neurotoxic phospholipases A_2 from Taiwan viper (*Vipera russelli formosensis*). *Eur J Biochem* **209**, 635–641.

146 Perbandt M, Tsai IH, Fuchs A, Banumathi S, Rajashankar KR, Georgieva D, Kalkura N, Singh TP, Genov N & Betzel C (2003) Structure of the heterodimeric neurotoxic complex viperotoxin F (RV-4/RV-7) from the venom of *Vipera russelli formosensis* at 1.9 Å resolution. *Acta Crystallogr D Biol Crystallogr* **59**, 1679–1687.

147 Kini RM & Chan YM (1999) Accelerated evolution and molecular surface of venom phospholipase A_2 enzymes. *J Mol Evol* **48**, 125–132.

148 Chang CC & Lee CY (1963) Isolation of neurotoxins from the venom of *Bungarus multicinctus* and their modes of neuromuscular blocking action. *Arch Int Pharmacodyn Ther* **144**, 241–257.

149 Bon C, Changeux JP, Jeng TW & Fraenkel-Conrat H (1979) Postsynaptic effects of crotoxin and of its isolated subunits. *Eur J Biochem* **99**, 471–481.

150 Chu CC, Li SH & Chen YH (1995) Resolution of iso-toxins in the beta-bungarotoxin family. *J Chromatogr A* **694**, 492–497.

151 Doley R & Kini RM (2009) Protein complexes in snake venom. *Cell Mol Life Sci* **66**, 2851–2871.

152 Kwong PD, McDonald NQ, Sigler PB & Hendrickson WA (1995) Structure of beta 2-bungarotoxin: potassium channel binding by Kunitz modules and targeted phospholipase action. *Structure* **3**, 1109–1119.

153 Neurath H (1984) Evolution of proteolytic enzymes. *Science* **224**, 350–357.

154 Birktoft JJ & Blow DM (1972) Structure of crystalline-chymotrypsin. V. The atomic structure of tosyl-chymotrypsin at 2 Å resolution. *J Mol Biol* **68**, 187–240.

155 Rawlings ND, Tolle DP & Barrett AJ (2004) MEROPS: the peptidase database. *Nucleic Acids Res* **32**, D160–D164.

156 Murakami MT & Arni RK (2005) Thrombomodulin-independent activation of protein C and specificity of hemostatically active snake venom serine proteinases: crystal structures of native and inhibited *Agkistrodon contortrix contortrix* protein C activator. *J Biol Chem* **280**, 39309–39315.

157 Marsh N & Williams V (2005) Practical applications of snake venom toxins in haemostasis. *Toxicon* **45**, 1171–1181.

158 Nakagaki T, Lin P & Kisiel W (1992) Activation of human factor VII by the prothrombin activator from the venom of *Oxyuranus scutellatus* (Taipan snake). *Thromb Res* **65**, 105–116.

159 Rosing J & Tans G (1991) Inventory of exogenous prothrombin activators. For the Subcommittee on Nomenclature of Exogenous Hemostatic Factors of the Scientific and Standardization Committee of the International Society on Thrombosis and Haemostasis. *Thromb Haemost* **65**, 627–630.

160 Bortoleto RK, Murakami MT, Watanabe L, Soares AM & Arni RK (2002) Purification, characterization and crystallization of Jararacussin-I, a fibrinogen-clotting enzyme isolated from the venom of *Bothrops jararacussu*. *Toxicon* **40**, 1307–1312.

161 Burkhart W, Smith GF, Su JL, Parikh I & LeVine H III (1992) Amino acid sequence determination of ancrod, the thrombin-like alpha-fibrinogenase from the venom of *Akistrodon rhodostoma*. *FEBS Lett* **297**, 297–301.

162 Itoh N, Tanaka N, Mihashi S & Yamashina I (1987) Molecular cloning and sequence analysis of cDNA for batroxobin, a thrombin-like snake venom enzyme. *J Biol Chem* **262**, 3132–3135.

163 Stocker K (1977) Defibrinogenation with thrombin-like snake venom enzymes. In *Handbook of Experimental Pharmacology* (Markwardt F, ed), pp. 451–484. Springer, Berlin.

164 Gempeler-Messina PM, Volz K, Buhler B & Muller C (2001) Protein C activators from snake venoms and their diagnostic use. *Haemostasis* **31**, 266–272.

165 Zhang Y, Wisner A, Xiong Y & Bon C (1995) A novel plasminogen activator from snake venom. Purification, characterization, and molecular cloning. *J Biol Chem* **270**, 10246–10255.

166 Liu S, Sun MZ & Greenaway FT (2006) A novel plasminogen activator from *Agkistrodon blomhoffii Ussurensis* venom (ABUSV-PA): purification and characterization. *Biochem Biophys Res Commun* **348**, 1279–1287.

167 Sanchez EF, Felicori LF, Chavez-Olortegui C, Magalhaes HB, Hermogenes AL, Diniz MV, Junqueira-de-Azevedo IL, Magalhaes A & Richardson M (2006) Biochemical characterization and molecular cloning of a plasminogen activator proteinase (LV-PA) from bushmaster snake venom. *Biochim Biophys Acta* **1760**, 1762–1771.

168 Zhang Y, Wisner A, Maroun RC, Choumet V, Xiong Y & Bon C (1997) *Trimeresurus stejnegeri* snake venom plasminogen activator. Site-directed mutagenesis and molecular modeling. *J Biol Chem* **272**, 20531–20537.

169 Epstein DM & Abeles RH (1992) Role of serine 214 and tyrosine 171, components of the S2 subsite of alpha-lytic protease, in catalysis. *Biochemistry* **31**, 11216–11223.

170 McGrath ME, Vasquez JR, Craik CS, Yang AS, Honig B & Fletterick RJ (1992) Perturbing the polar environment of Asp102 in trypsin: consequences of replacing conserved Ser214. *Biochemistry* **31**, 3059–3064.

171 Schechter I & Berger A (1967) On the size of the active site in proteases. I. Papain. *Biochem Biophys Res Commun* **27**, 157–162.

172 Perona JJ & Craik CS (1995) Structural basis of substrate specificity in the serine proteases. *Protein Sci* **4**, 337–360.

173 Huber R & Bode W (1978) Structural basis of the activation and action of trypsin. *Acc Chem Res* **11**, 114–122.

174 Kisiel W, Kondo S, Smith KJ, McMullen BA & Smith LF (1987) Characterization of a protein C activator from *Agkistrodon contortrix contortrix* venom. *J Biol Chem* **262**, 12607–12613.

175 Parry MA, Jacob U, Huber R, Wisner A, Bon C & Bode W (1998) The crystal structure of the novel snake venom plasminogen activator TSV-PA: a prototype structure for snake venom serine proteinases. *Structure* **6**, 1195–1206.

176 Zhu Z, Liang Z, Zhang T, Xu W, Teng M & Niu L (2005) Crystal structures and amidolytic activities of two glycosylated snake venom serine proteinases. *J Biol Chem* **280**, 10524–10529.

177 Bode W, Schwager P & Huber R (1978) The transition of bovine trypsinogen to a trypsin-like state upon strong ligand binding. The refined crystal structures of the bovine trypsinogen-pancreatic trypsin inhibitor complex and of its ternary complex with Ile-Val at 1.9 Å resolution. *J Mol Biol* **118**, 99–112.

178 Hedstrom L, Lin TY & Fast W (1996) Hydrophobic interactions control zymogen activation in the trypsin family of serine proteases. *Biochemistry* **35**, 4515–4523.

179 Joseph JS, Chung MC, Jeyaseelan K & Kini RM (1999) Amino acid sequence of trocarin, a prothrombin activator from *Tropidechis carinatus* venom: its structural similarity to coagulation factor Xa. *Blood* **94**, 621–631.

180 Masci PP, Whitaker AN & de Jersey J (1988) Purification and characterization of a prothrombin activator from the venom of the Australian brown snake, *Pseudonaja textilis textilis*. *Biochem Int* **17**, 825–835.

181 Rao VS & Kini RM (2002) Pseutarin C, a prothrombin activator from *Pseudonaja textilis* venom: its structural and functional similarity to mammalian coagulation factor Xa–Va complex. *Thromb Haemost* **88**, 611–619.

182 Rao VS, Swarup S & Kini RM (2003) The nonenzymatic subunit of pseutarin C, a prothrombin activator from eastern brown snake (*Pseudonaja textilis*) venom, shows structural similarity to mammalian coagulation factor V. *Blood* **102**, 1347–1354.

183 Rao VS, Swarup S & Kini RM (2004) The catalytic subunit of pseutarin C, a group C prothrombin activator from the venom of *Pseudonaja textilis*, is structurally similar to mammalian blood coagulation factor Xa. *Thromb Haemost* **92**, 509–521.

184 Minh Le TN, Reza MA, Swarup S & Kini RM (2005) Gene duplication of coagulation factor V and origin of venom prothrombin activator in *Pseudonaja textilis* snake. *Thromb Haemost* **93**, 420–429.

185 Reza A, Swarup S & Kini RM (2005) Two parallel prothrombin activator systems in Australian rough-scaled snake, *Tropidechis carinatus*. Structural comparison of venom prothrombin activator with blood coagulation factor X. *Thromb Haemost* **93**, 40–47.

186 Reza MA, Minh Le TN, Swarup S & Kini RM (2006) Molecular evolution caught in action: gene duplication and evolution of molecular isoforms of prothrombin activators in *Pseudonaja textilis* (brown snake). *J Thromb Haemost* **4**, 1346–1353.

187 Reza MA, Swarup S & Kini RM (2007) Structure of two genes encoding parallel prothrombin activators in *Tropidechis carinatus* snake: gene duplication and recruitment of factor X gene to the venom gland. *J Thromb Haemost* **5**, 117–126.

188 Fox JW & Serrano SM (2008) Insights into and speculations about snake venom metalloproteinase (SVMP) synthesis, folding and disulfide bond formation and their contribution to venom complexity. *FEBS J* **275**, 3016–3030.

189 Fox JW & Serrano SM (2005) Structural considerations of the snake venom metalloproteinases, key members of the M12 reprolysin family of metalloproteinases. *Toxicon* **45**, 969–985.

190 Edwards DR, Handsley MM & Pennington CJ (2009) The ADAM metalloproteinases. *Mol Aspects Med* **29**, 258–289.

191 Murphy G (2008) The ADAMs: signalling scissors in the tumour microenvironment. *Nat Rev Cancer* **8**, 929–941.

192 Blobel CP (2005) ADAMs: key components in EGFR signalling and development. *Nat Rev Mol Cell Biol* **6**, 32–43.

193 Mochizuki S & Okada Y (2007) ADAMs in cancer cell proliferation and progression. *Cancer Sci* **98**, 621–628.

194 Moss ML, Jin SL, Milla ME, Bickett DM, Burkhart W, Carter HL, Chen WJ, Clay WC, Didsbury JR, Hassler D *et al.* (1997) Cloning of a disintegrin metalloproteinase that processes precursor tumour-necrosis factor-alpha. *Nature* **385**, 733–736.

195 Black RA, Rauch CT, Kozlosky CJ, Peschon JJ, Slack JL, Wolfson MF, Castner BJ, Stocking KL, Reddy P, Srinivasan S *et al.* (1997) A metalloproteinase disintegrin that releases tumour-necrosis factor-alpha from cells. *Nature* **385**, 729–733.

196 Porter S, Clark IM, Kevorkian L & Edwards DR (2005) The ADAMTS metalloproteinases. *Biochem J* **386**, 15–27.

197 Apte SS (2009) A disintegrin-like and metalloprotease (reprolysin-type) with thrombospondin type 1 motif (ADAMTS) superfamily-functions and mechanisms. *J Biol Chem* **284**, 31493–31497.

198 Gerhardt S, Hassall G, Hawtin P, McCall E, Flavell L, Minshull C, Hargreaves D, Ting A, Pauptit RA, Parker AE *et al.* (2007) Crystal structures of human ADAMTS-1 reveal a conserved catalytic domain and a disintegrin-like domain with a fold homologous to cysteine-rich domains. *J Mol Biol* **373**, 891–902.

199 Mosyak L, Georgiadis K, Shane T, Svenson K, Hebert T, McDonagh T, Mackie S, Olland S, Lin L, Zhong X *et al.* (2008) Crystal structures of the two major aggrecan degrading enzymes, ADAMTS4 and ADAMTS5. *Protein Sci* **17**, 16–21.

200 Akiyama M, Takeda S, Kokame K, Takagi J & Miyata T (2009) Crystal structures of the non-catalytic domains of ADAMTS13 reveal multiple discontinuous exosites for von Willebrand factor. *Proc Natl Acad Sci USA* **106**, 19274–19279.

201 Takeda S (2009) Three-dimensional domain architecture of the ADAM family proteinases. *Semin Cell Dev Biol* **20**, 146–152.

202 Gomis-Ruth FX, Kress LF & Bode W (1993) First structure of a snake venom metalloproteinase: a proto-

type for matrix metalloproteinases/collagenases. *EMBO J* **12**, 4151–4157.

203 Gomis-Ruth FX, Kress LF, Kellermann J, Mayr I, Lee X, Huber R & Bode W (1994) Refined 2.0 Å X-ray crystal structure of the snake venom zinc-endo-peptidase adamalysin II. Primary and tertiary structure determination, refinement, molecular structure and comparison with astacin, collagenase and thermolysin. *J Mol Biol* **239**, 513–544.

204 Masuda S, Hayashi H & Araki S (1998) Two vascular apoptosis-inducing proteins from snake venom are members of the metalloprotease/disintegrin family. *Eur J Biochem* **253**, 36–41.

205 Masuda S, Ohta T, Kaji K, Fox JW, Hayashi H & Araki S (2000) cDNA cloning and characterization of vascular apoptosis-inducing protein 1. *Biochem Biophys Res Commun* **278**, 197–204.

206 Takeda S, Igarashi T, Mori H & Araki S (2006) Crystal structures of VAP1 reveal ADAMs' MDC domain architecture and its unique C-shaped scaffold. *EMBO J* **25**, 2388–2396.

207 Takeda S (2010) VAP1: snake venom homolog of mammalian ADAMs. In *Handbook of Metalloproteins* (Messerschmidt A ed), Vol. 5, 699–671. Wiley, Chichester.

208 Lingott T, Schleberger C, Gutierrez JM & Merfort I (2009) High-resolution crystal structure of the snake venom metalloproteinase BaP1 complexed with a pepti-domimetic: insight into inhibitor binding. *Biochemistry* **48**, 6166–6174.

209 Gutierrez JM, Rucavado A, Escalante T & Diaz C (2005) Hemorrhage induced by snake venom metallo-proteinases: biochemical and biophysical mechanisms involved in microvessel damage. *Toxicon* **45**, 997–1011.

210 Igarashi T, Araki S, Mori H & Takeda S (2007) Crystal structures of catrocollastatin/VAP2B reveal a dynamic, modular architecture of ADAM/adamaly-sin/reprolysin family proteins. *FEBS Lett* **581**, 2416–2422.

211 Takeda S, Igarashi T & Mori H (2007) Crystal structure of RVV-X: An example of evolutionary gain of specificity by ADAM proteinases. *FEBS Lett* **581**, 5859–5864.

212 Liu H, Shim AH & He X (2009) Structural character-ization of the ectodomain of a disintegrin and metallo-proteinase-22 (ADAM22), a neural adhesion receptor instead of metalloproteinase: insights on ADAM func-tion. *J Biol Chem* **284**, 29077–29086.

213 Fujii Y, Okuda D, Fujimoto Z, Horii K, Morita T & Mizuno H (2003) Crystal structure of trimestatin, a dis-integrin containing a cell adhesion recognition motif RGD. *J Mol Biol* **332**, 1115–1122.

214 Calvete JJ, Marcinkiewicz C, Monleon D, Esteve V, Celda B, Juarez P & Sanz L (2005) Snake venom disin-tegrins: evolution of structure and function. *Toxicon* **45**, 1063–1074.

215 Janes PW, Saha N, Barton WA, Kolev MV, Wimmer-Kleikamp SH, Nievergall E, Blobel CP, Himanen JP, Lackmann M & Nikolov DB (2005) Adam meets Eph: an ADAM substrate recognition module acts as a molecular switch for ephrin cleavage in trans. *Cell* **123**, 291–304.

216 Marchler-Bauer A, Anderson JB, Chitsaz F, Derby-shire MK, DeWeese-Scott C, Fong JH, Geer LY, Geer RC, Gonzales NR, Gwadz M *et al.* (2009) CDD: spe-cific functional annotation with the Conserved Domain Database. *Nucleic Acids Res* **37**, D205–210.

217 Takeya H, Nishida S, Miyata T, Kawada S, Saisaka Y, Morita T & Iwanaga S (1992) Coagulation factor X activating enzyme from Russell's viper venom (RVV-X). A novel metalloproteinase with disintegrin (platelet aggregation inhibitor)-like and C-type lectin-like domains. *J Biol Chem* **267**, 14109–14117.

218 Gowda DC, Jackson CM, Hensley P & Davidson EA (1994) Factor X-activating glycoprotein of Russell's viper venom. Polypeptide composition and character-ization of the carbohydrate moieties. *J Biol Chem* **269**, 10644–10650.

219 Morita T (1998) Proteases which activate factor X. In *Enzymes from Snake Venom* (Bailey GS ed), pp. 179–208. Alaken, Ft Collins, CO.

220 Tans G & Rosing J (2001) Snake venom activators of factor X: an overview. *Haemostasis* **31**, 225–233.

221 Atoda H, Ishikawa M, Mizuno H & Morita T (1998) Coagulation factor X-binding protein from *Deinagkistr-odon acutus* venom is a Gla domain-binding protein. *Biochemistry* **37**, 17361–17370.

222 Mizuno H, Fujimoto Z, Atoda H & Morita T (2001) Crystal structure of an anticoagulant protein in com-plex with the Gla domain of factor X. *Proc Natl Acad Sci USA* **98**, 7230–7234.

223 Takeda S (2010) Structural aspects of the factor X acti-vator RVV-X from Russell's viper venom. In *Toxins and Hemostasis: From Bench to Bedside* (Kini R, Clemetson KJ, Markland FS, McLane MA & Morita T eds), pp. 465–484. Springer Science + Business Media, London.

224 Usami Y, Fujimura Y, Miura S, Shima H, Yoshida E, Yoshioka A, Hirano K, Suzuki M & Titani K (1994) A 28 kDa-protein with disintegrin-like structure (jararha-gin-C) purified from *Bothrops jararaca* venom inhibits collagen- and ADP-induced platelet aggregation. *Biochem Biophys Res Commun* **201**, 331–339.

225 Shimokawa K, Shannon JD, Jia LG & Fox JW (1997) Sequence and biological activity of catrocollastatin-C: a disintegrin-like/cysteine-rich two-domain protein from *Crotalus atrox* venom. *Arch Biochem Biophys* **343**, 35–43.

226 Limam I, Bazaa A, Srairi-Abid N, Taboubi S, Jebali J, Zouari-Kessentini R, Kallech-Ziri O, Mejdoub H, Hammami A, El Ayeb M *et al.* (2010) Leberagin-C,

a disintegrin-like/cysteine-rich protein from *Macrovipera lebetina transmediterranea* venom, inhibits alphavbeta3 integrin-mediated cell adhesion. *Matrix Biol* **29**, 117–126.

227 Selistre-de-Araujo HS, Cominetti MR, Terruggi CH, Mariano-Oliveira A, De Freitas MS, Crepin M, Figueiredo CC & Morandi V (2005) Alternagin-C, a disintegrin-like protein from the venom of *Bothrops alternatus*, modulates alpha2beta1 integrin-mediated cell adhesion, migration and proliferation. *Braz J Med Biol Res* **38**, 1505–1511.

228 Jia LG, Wang XM, Shannon JD, Bjarnason JB & Fox JW (2000) Inhibition of platelet aggregation by the recombinant cysteine-rich domain of the hemorrhagic snake venom metalloproteinase, atrolysin A. *Arch Biochem Biophys* **373**, 281–286.

229 Serrano SM, Jia LG, Wang D, Shannon JD & Fox JW (2005) Function of the cysteine-rich domain of the haemorrhagic metalloproteinase atrolysin A: targeting adhesion proteins collagen I and von Willebrand factor. *Biochem J* **391**, 69–76.

230 Serrano SM, Wang D, Shannon JD, Pinto AF, Polanowska-Grabowska RK & Fox JW (2007) Interaction of the cysteine-rich domain of snake venom metalloproteinases with the A1 domain of von Willebrand factor promotes site-specific proteolysis of von Willebrand factor and inhibition of von Willebrand factor-mediated platelet aggregation. *FEBS J* **274**, 3611–3621.

231 Serrano SM, Kim J, Wang D, Dragulev B, Shannon JD, Mann HH, Veit G, Wagener R, Koch M & Fox JW (2006) The cysteine-rich domain of snake venom metalloproteinases is a ligand for von Willebrand factor A domains: role in substrate targeting. *J Biol Chem* **281**, 39746–39756.

232 Menezes MC, Paes Leme AF, Melo RL, Silva CA, Della Casa M, Bruni FM, Lima C, Lopes-Ferreira M, Camargo AC, Fox JW *et al.* (2008) Activation of leukocyte rolling by the cysteine-rich domain and the hyper-variable region of HF3, a snake venom hemorrhagic metalloproteinase. *FEBS Lett* **582**, 3915–3921.

233 Kamiguti AS, Gallagher P, Marcinkiewicz C, Theakston RD, Zuzel M & Fox JW (2003) Identification of sites in the cysteine-rich domain of the class P-III snake venom metalloproteinases responsible for inhibition of platelet function. *FEBS Lett* **549**, 129–134.

234 Guan HH, Goh KS, Davamani F, Wu PL, Huang YW, Jeyakanthan J, Wu WG & Chen CJ (2009) Structures of two elapid snake venom metalloproteases with distinct activities highlight the disulfide patterns in the D domain of ADAMalysin family proteins. *J Struct Biol* **169**, 294–303.

235 Morita T (2005) Structures and functions of snake venom CLPs (C-type lectin-like proteins) with

anticoagulant-, procoagulant-, and platelet-modulating activities. *Toxicon* **45**, 1099–1114.

236 Arnold K, Bordoli L, Kopp J & Schwede T (2006) The SWISS-MODEL workspace: a web-based environment for protein structure homology modelling. *Bioinformatics* **22**, 195–201.

237 Guex N & Peitsch MC (1997) SWISS-MODEL and the Swiss-PdbViewer: an environment for comparative protein modeling. *Electrophoresis* **18**, 2714–2723.

238 Berman HM, Westbrook JD, Gabanyi MJ, Tao W, Shah R, Kouranov A, Schwede T, Arnold K, Kiefer F, Bordoli L *et al.* (2009) The protein structure initiative structural genomics knowledgebase. *Nucleic Acids Res* **37**, D365–368.

239 Colletier JP, Fournier D, Greenblatt HM, Stojan J, Sussman JL, Zaccai G, Silman I & Weik M (2006) Structural insights into substrate traffic and inhibition in acetylcholinesterase. *EMBO J* **25**, 2746–2756.

240 Patrick GL (2001) *An Introduction to Medicinal Chemistry. Cholinergics, Anticholinergics, and Anticholinesterase.* Oxford University Press, Oxford.

Supporting information

The following supplementary material is available:

Fig. S1. Sequence alignment of groups I and II PLA$_2$s.

Fig. S2. (A) Disulfide connectivity of group I PLA$_2$. (B) Overall fold of group I PLA$_2$ showing α-helices as cylinders and β-strands as arrows.

Fig. S3. (A) Disulfide connectivity of group II PLA$_2$. (B) Overall fold of group II PLA$_2$ chain.

Fig. S4. The six subsites of PLA$_2$.

Fig. S5. The residues of PLA$_2$ involved in catalysis.

Fig. S6. Structures of PLA$_2$ with (A) aristolochic acid (B) vitamin E and (C) atropine to PLA$_2$.

Fig. S7. Structures of PLA$_2$ with indole molecules and their derivatives.

Fig. S8. Structures of PLA$_2$ with NSAIDS: (A) oxyphenbutazone (B) diclofenac (C) indomethacin binds to PLA$_2$ in a different mode.

Table S1. Selection of the X-ray structures of SVMPs, ADAMs and ADAMTSs deposited in the PDB.

This supplementary material can be found in the online version of this article.

Please note: As a service to our authors and readers, this journal provides supporting information supplied by the authors. Such materials are peer-reviewed and may be re-organized for online delivery, but are not copy-edited or typeset. Technical support issues arising from supporting information (other than missing files) should be addressed to the authors.